DEVELOPMENT OF SUPERHYDROPHOBIC AND TRANSPARENT COATING

By:

Ahmad Shahbaz

Amna Shahid

Hashir Akram

School of Chemical and Materials Engineering

National University of Sciences and Technology

2023

DEVELOPMENT OF SUPERHYDROPHOBIC AND TRANSPARENT COATING

By

Leader- Ahmad Shahbaz (296125)

Member 1- Amna Shahid (289824)

Member 2- Hashir Akram (289125)

A Thesis Submitted as partial fulfillment of the requirements for the degree of

BE in (Materials and Metallurgical Engineering)

Supervisor: Dr. Muhammad Shoaib Butt
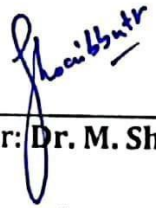
Co-Supervisor: Dr. Muhmmad Irfan

School of Chemical and Materials Engineering (SCME)

National University of Sciences and Technology (NUST)
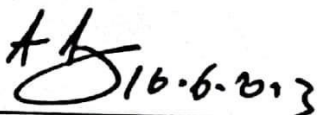
June, 2023

CERTIFICATE

This is to certify that work in this thesis has been completed by **Mr. Ahmad Shahbaz, Ms. Amna Shahid,** and **Mr. Hashir Akram** under the supervision of Dr. Muhammad Shoaib Butt and Dr. Muhammad Irfan at the School of Chemical and Materials Engineering (SCME), National University of Sciences and Technology, H-12, Islamabad, Pakistan.

Supervisor: **Dr. M. Shoaib Butt**

Department of Materials Engineering

School of Chemical and Materials Engineering

National University of Sciences and Technology, Islamabad

Co-Supervisor: **Dr. M. Irfan**

Department of Materials Engineering

School of Chemical and Materials Engineering

National University of Sciences and Technology

Submitted through:

HOD: **Dr. Khurram Yaqoob**   16/06/23

Department of Materials Engineering
School of Chemical and Materials Engineering
National University of Sciences and Technology, Islamabad

Principal/Dean: Prof **Dr. Amir Azam Khan**   16.6.23

School of Chemical and Materials Engineering
National University of Sciences and Technology

DEDICATION

With profound reverence,

*We express our heartfelt dedication to our **dear parents** and **esteemed teachers**, whose unwavering guidance and support were invaluable throughout this project.*

ACKNOWLEDGEMENTS

ABSTRACT

  The goal of this study is to create a transparent superhydrophobic coating that has been specially designed for usage in automotive applications. The goal is to treat the problems brought on by water collection on car bodies, such as corrosion, wear, and scratches, while making sure the paint's integrity is not jeopardized. The three major goals of the research are to synthesize a transparent superhydrophobic coating material, analyze its properties using multiple methods, and apply the coating to mild steel substrates. To accomplish the first goal, a superhydrophobic clear coating material is created by carefully choosing and combining appropriate components while taking transparency and other aspects like hydrophobicity into account. To ensure reproducibility and scalability, the reaction conditions and composition are optimized for the synthesis of the material.

To achieve the second goal, modern characterization methods like Fourier-transform infrared spectroscopy (FTIR), scanning electron microscopy (SEM), and contact angle measurements are used to examine the properties of the synthesized coating material. For further optimization and evaluation, this study offers vital insights into the material's chemical structure, shape, and wettability. The third goal is to apply the created superhydrophobic transparent coating to mild steel substrates, which are frequently used in car bodies. Considerations such as coating material qualities and required thickness are considered when examining coating deposition processes such as spray coating, dip coating, or electrophoretic deposition (EPD). To assess super hydrophobicity, transparency, adhesion, and durability, the coated mild steel samples are put through stringent performance testing.

The findings of this study have important applications in the automotive industry, providing a way to reduce corrosion, wear, and scratches brought on by water collection while preserving the car's aesthetic appeal. The creation of a

transparent superhydrophobic coating improves the surface integrity, durability, and performance of vehicles while also increasing their aesthetic appeal.

TABLE OF CONTENTS

LIST OF FIGURES

<div align="right">**CHAPTER 1**</div>

INTRODUCTION

1.1 Solving automotive problems

The development of superhydrophobic and transparent coatings specifically tailored for automotive applications has garnered significant attention in recent years. The automotive industry is continuously seeking innovative solutions to enhance vehicle performance, safety, and aesthetics [3]. Superhydrophobic and transparent coatings offer a promising avenue to address some of the challenges faced by vehicles in terms of water repellency, visibility, and surface protection [6].

Superhydrophobic coatings exhibit exceptional water repellency, preventing water droplets from adhering to surfaces and forming a film. This property is derived from the unique micro- and nanostructures present on the coating surface, which mimic natural water-repellent surfaces such as lotus leaves. By effectively repelling water, these coatings help to maintain a clear view through windshields and side mirrors, especially during rainy conditions, thereby significantly improving driver visibility and safety.

Transparency is another crucial requirement for automotive coatings. The ability to maintain optical clarity without compromising the underlying substrate is essential for various applications, including windows, headlights, and taillights. Transparent coatings must allow maximum light transmission, ensuring optimal visibility for both drivers and pedestrians, while also providing a protective barrier against environmental factors such as UV radiation, dirt, and scratches [28].

The development of superhydrophobic and transparent coatings for automotive applications involves a multidisciplinary approach. Researchers and engineers combine principles from materials science, surface chemistry, nanotechnology, and coating technologies to create coatings that exhibit the desired properties. Advanced fabrication techniques, such as sol-gel processes, chemical vapor

deposition, and plasma-enhanced techniques, are utilized to deposit the coatings onto automotive surfaces. The selection of appropriate materials and optimization of coating thickness and surface morphology are critical factors that impact the performance and durability of the coatings.

The automotive industry stands to benefit greatly from the implementation of superhydrophobic and transparent coatings. Improved water repellency on windshields and side mirrors can enhance driver visibility and safety by reducing water droplet adhesion and maintaining a clear view. Furthermore, the use of transparent coatings on windows, headlights, and taillights provides long-lasting protection against environmental factors while ensuring optimal light transmission and visual aesthetics.

In addition to improving safety and aesthetics, superhydrophobic and transparent coatings offer potential energy-saving benefits for vehicles. By repelling water, these coatings minimize the accumulation of moisture, ice, and snow on the vehicle's exterior, reducing the weight burden and improving aerodynamic efficiency. This, in turn, can contribute to fuel efficiency and overall performance.

This topic focuses on the ongoing research and development efforts in creating superhydrophobic and transparent coatings specifically tailored for automotive applications. It explores the underlying scientific principles, fabrication techniques, and characterization methods used to achieve the desired properties. The potential benefits, challenges, and prospects of implementing these coatings in the automotive industry are also discussed, highlighting the significant impact they can have on vehicle performance, safety, and sustainability.

1.2 Selection of Material

1.2.1 Selection of Resin

There are several options to consider while developing a transparent, hydrophobic coating for automotive applications. Here is a thorough comparison of two substitutes, acrylic resin, and fluoropolymer, with melamine formaldehyde resin, with an emphasis on availability and cost:

Melamine Formaldehyde Resin:

Melamine formaldehyde resins are generally accessible on the market and are simple to obtain from a variety of sources. They are a well-known and widely available alternative because they have been used for a long time in many industries, including automobile coatings [1].

Cost:

When compared to some other specialized resins, melamine formaldehyde resins are typically more affordable. Their significantly cheaper cost is a result of the availability of raw materials and well-established manufacturing techniques. Because of this, melamine formaldehyde resin is an economical option for extensive automotive applications.

Acrylic Resin:

Availability: Acrylic resins are widely used in the coatings industry, particularly automotive coatings. They are also easily accessible. They are created through the polymerization of easily available acrylic monomers from the market. Multiple vendors can supply acrylic resins, providing good availability [19].

Cost:

The price of acrylic resins varies according to the formulation and quality. Acrylic resins are typically thought of as being reasonably priced. However, the price may go up if specialized formulations or additives are needed to attain qualities like hydrophobicity or transparency.

Fluoropolymer:

Availability: Due to their outstanding hydrophobic qualities, fluoropolymers like polytetrafluoroethylene (PTFE) and polyvinylidene fluoride (PVDF) are frequently employed in specialized coatings. Compared to melamine formaldehyde and acrylic resins, the selection of acceptable fluoropolymers for automotive coatings may be more constrained despite their widespread availability [8].

Cost:

In general, fluoropolymers are more expensive than acrylic resins and melamine formaldehyde. Fluoropolymer coatings are more expensive due to their specialized nature and the comparatively high cost of their raw components. The overall viability of using fluoropolymers in extensive automotive applications may be impacted by this cost increase.

Melamine formaldehyde resin stands out as a top choice for creating a transparent, hydrophobic coating for automotive applications after a thorough evaluation of costs and availability. Due to its widespread accessibility from numerous vendors, it has good availability. Melamine formaldehyde resin is very economical, making it appropriate for mass production without greatly raising the cost of the coating overall. Melamine formaldehyde resin is the greatest option for automotive applications in terms of overall practicality and feasibility, but acrylic resins and fluoropolymers are also viable alternatives. This is because it combines the desired qualities with an ideal balance of availability and cost.

1.2.2 Selection of Reinforcement

1.2.2.1   Silica nanoparticles:

It can be a very good choice for improving a coating's ability to become superhydrophobic. To see why silica nanoparticles are the greatest option, let us contrast them with two other viable options, namely fluorinated substances, and carbon-based nanomaterials:

Effectiveness: Silica nanoparticles have been thoroughly investigated and shown to improve coatings' hydrophobicity. They have a large surface area and can be altered to add functional groups that are hydrophobic to their surfaces, which results in great water repellency. Better surface roughness is made possible by the nanostructure of silica particles, which is essential for obtaining super hydrophobicity [6].

Availability: There are several suppliers who supply silica nanoparticles in the market, and they come in a range of sizes and surface treatments. They are easily accessible for integration into coating formulations due to their popularity and availability in sectors including coatings, paints, and additives.

Cost: In comparison to other nanomaterials, silica nanoparticles are rather affordable. Their affordable price is a result of the plentiful supply of raw ingredients (silica) and well-established manufacturing techniques. Because of their accessibility, they are a sensible option for mass production.

Effectiveness of Fluorinated Compounds: Hydrophobic properties of fluorinated compounds, such as those of fluoroalkyl silanes, are well recognized. They can provide coatings high water repellency. However, depending on the precise formulation and administration technique, fluorinated chemicals' efficacy can vary. Additionally, given that fluorinated chemicals can degrade over time, the durability of their hydrophobic properties might be a problem.

Fluorinated chemicals are typically offered on the market, however compared to silica nanoparticles, their variety may be more constrained. Moreover, achieving the desired formulation may involve additional modification or sourcing difficulties depending on the fluorinated component and its application needs.

Cost: In comparison to silica nanoparticles, fluorinated chemicals are frequently more expensive. These compounds are more expensive due to their specialized character and the high cost of their basic components. The overall viability of employing fluorinated chemicals, particularly for large-scale coating applications, may be impacted by this cost increase.

1.2.2.2   Nanomaterials Based on Carbon:

Effectiveness: Hydrophobic coatings have been investigated for carbon-based nanomaterials including carbon nanotubes and graphene. Despite having excellent qualities, they could not be as effective as silica nanoparticles at achieving super hydrophobicity. The difficulty lies in achieving the desired surface roughness and homogenous dispersion, both of which are necessary for efficient water repellency.

Carbon-based nanomaterials are becoming more widely available on the market, but they may still have more limited availability and industrial scalability than silica nanoparticles. Their specialized character and requirement for manufacturing methods may prevent them from being widely used.

Cost: Due to their intricate synthesis procedures and the high price of raw materials, carbon-based nanomaterials often tend to be more expensive than silica nanoparticles. Their suitability for large-scale coating applications may be constrained by their higher cost. Based on the comparison, silica nanoparticles stand out as the top choice for coatings that want to have superhydrophobic qualities. They are highly efficient at increasing hydrophobicity, readily available from a variety of vendors, and reasonably priced. While carbon-based nanomaterials and fluorinated chemicals also have advantages, silica nanoparticles offer a tried-and-true method for making superhydrophobic coatings that is also inexpensive and widely available. The best option for adding into coatings to create super hydrophobicity is silica nanoparticles due to their effectiveness, availability, and cost-effectiveness.

1.3 Proposed Material

1.3.1 Melamine Formaldehyde

Melamine formaldehyde (MF) is a thermosetting resin that is formed by the reaction between melamine and formaldehyde. It is commonly used in a wide range of industries, including construction, furniture manufacturing, automotive, and electronics.

It is obtained from the reaction between melamine, which is a white crystalline powder and formaldehyde, which is a colorless liquid that aids in cross-linking of melamine [14].
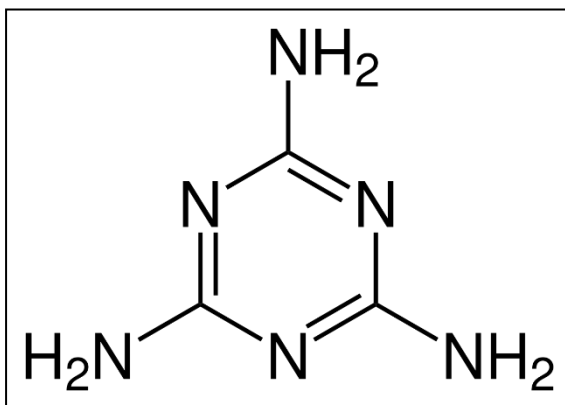
Figure 1, Melamine
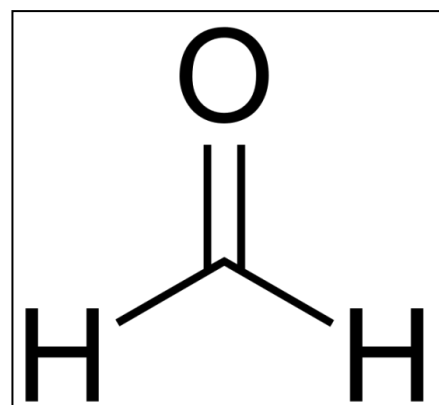
Figure 2, Formaldehyde
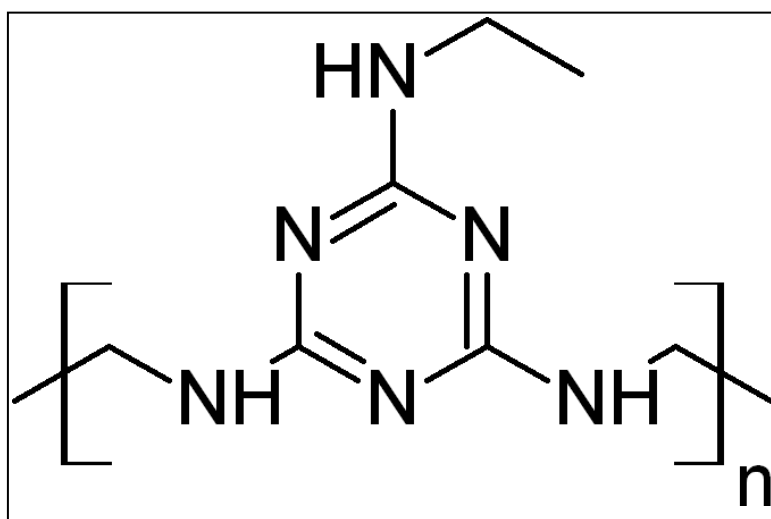
Figure 3, Structural formula of melamine formaldehyde.

1.3.2 Silica nanoparticles

Silicon dioxide (SiO_2), sometimes referred to as silica, makes up most of the nanoscale particles known as silica nanoparticles. Their compact size and high surface area to volume ratio provide them special features and make them suitable for use in a variety of industries [32].

There are various ways to make silica nanoparticles, including sol-gel procedures, precipitation, and aerosol approaches. The size, shape, and surface characteristics of the nanoparticles may be precisely controlled using these techniques. Silica nanoparticles typically range in size from 1 to 100 nanometers.

Silica nanoparticles' surfaces can be altered to modify their characteristics for certain uses. To improve their stability, dispersibility, or compatibility with other materials, surfaces can be modified by adding different surface coatings or functionalizing them with organic molecules.

Due to their small size and large surface area, silica nanoparticles exhibit unique physical and chemical properties. They possess excellent thermal stability, high mechanical strength, and optical transparency, making them suitable for a wide range of applications.

The property which was of the most interest in this research was the super hydrophobicity imparted by silica nanoparticles.

1.4 Problem Statement

Water buildup on car bodies is a serious problem since it causes corrosion, accelerates wear, causes scratches, and jeopardizes the paint's integrity. These problems compromise the vehicle's structural integrity and shorten its lifespan in addition to affecting its aesthetic appeal. Traditional coatings frequently do not offer enough protection, and because they are opaque, they change how the car looks. As a result, there is a critical need for the creation of a transparent coating with superhydrophobic qualities to successfully prevent corrosion, reduce wear, and maintain the quality of the car's paint [16]. The following primary research questions are the focus of the problem statement for this thesis:

How can a transparent superhydrophobic coating be created to stop water from collecting on car bodies?

What properties and chemical makeup of materials are necessary to create super hydrophobicity and transparency?

What coating deposition methods may be used to guarantee the homogeneity and adhesion of the transparent superhydrophobic coating on various automotive surfaces?

How well does the coating work in terms of preventing corrosion, reducing wear, and preventing scratches?

How can the created coating be practically applied in the automobile sector to increase the durability and appeal of vehicles while preserving the original paint quality?

This thesis seeks to offer a thorough understanding of the creation, functionality, and real-world applications of a superhydrophobic transparent coating for automobiles by addressing these research questions. The results of this study will revolutionize automotive coatings by offering a practical way to reduce corrosion, wear, and scratches brought on by water accumulation while maintaining the aesthetic value and paint integrity of vehicles.

1.5 Objectives

Creating a superhydrophobic transparent coating material is the first goal.

The project's primary goal is to create a transparent superhydrophobic coating material that is acceptable for the intended application. This goal entails investigating various chemical formulations and compositions to create a coating material that possesses exceptional superhydrophobic qualities while retaining transparency. To attain the desired properties, the synthesis process may entail the selection and blending of numerous ingredients, such as polymers, nanoparticles, or additives. Optimizing the synthesis parameters, such as reaction conditions, temperature, and reaction time, is one of the goals to assure the reproducibility and scalability of the synthesis of coating materials. The goal is to set the stage for more research and coating development by successfully synthesizing the superhydrophobic transparent coating material.

Using a variety of techniques, analyze the properties of coating materials

The second goal focuses on applying a variety of characterization techniques to examine the properties of the synthesized coating material. Utilizing methods like Fourier-transform infrared spectroscopy (FTIR), scanning electron microscopy (SEM), optical profilometry, optical microscopy and contact angle measurements is necessary to achieve this. These methods offer insightful information about the coating material's chemical composition, shape, surface topography, and wettability. The goal is to get a thorough understanding of the structure, composition, and surface interactions of the coating material by the investigation of these aspects. This information is essential for further optimizing the coating material and determining its applicability.

Application of a coating on mild steel substrate.

The third goal is to coat mild steel substrates with the synthesized superhydrophobic transparent coating. To achieve this goal, a suitable coating deposition process must be chosen, such as electrophoretic deposition (EPD), dip coating, or spray coating, depending on the features of the substrate, the coating material, and the required coating thickness. To achieve homogenous and adherent coatings, the coating process will be optimized by modifying variables

such coating solution concentration, drying conditions, and curing techniques. Several performance tests will be performed on the coated mild steel samples to measure the coating's super hydrophobicity, transparency, adhesion, and durability. This goal is to show that the synthetic coating material can be successfully applied to mild steel substrates, opening the door for future applications in corrosion prevention and surface improvement.

These goals are further developed in the project, which intends to synthesize a superhydrophobic transparent coating material, effectively apply the coating to mild steel substrates, and analyze the material's properties using a variety of methods. These goals add up to the creation of an efficient coating solution that combines super hydrophobicity, transparency, and durability for uses in mild steel surface enhancement and corrosion protection.

CHAPTER 2

LITERATURE REVIEW

2.1 Introduction:

Superhydrophobic coatings for steel surfaces are designed to impart exceptional water-repellent properties. Super hydrophobicity refers to the ability of a surface to repel water droplets and maintain a high contact angle with water. In the context of steel coatings, super hydrophobicity offers several benefits, including enhanced corrosion resistance, self-cleaning properties, and improved durability [6].

Superhydrophobic coatings are typically composed of a combination of hydrophobic (water-repellent) materials and nanostructures that create a rough surface texture. These materials can include polymers, nanoparticles, and functional molecules. The coating is applied to the steel surface using various techniques such as spraying, dip coating, or spin coating.

Overall, the developed superhydrophobic coating on steel surfaces, characterized by its self-cleaning, anti-fogging, and anti-corrosion properties, holds great potential for a wide range of industrial applications [5].

The unique surface structure created by the superhydrophobic coating prevents water from spreading on the surface. Instead, water droplets tend to bead up and roll off the surface, carrying away dirt and contaminants. This self-cleaning effect helps to maintain the cleanliness and aesthetics of the steel surface [28].

In addition to self-cleaning, superhydrophobic coatings offer improved corrosion resistance. By repelling water, the coatings prevent moisture from directly contacting the steel surface. Since corrosion requires the presence of both water and oxygen, minimizing water contact helps reduce the chances of rust formation and corrosion.

Superhydrophobic coatings also enhance the durability and lifespan of steel. They act as a protective barrier against harsh environmental conditions,

including exposure to chemicals, UV radiation, and abrasion. By providing an additional layer of defense, the coatings can significantly extend the service life of steel components and structures.

Furthermore, superhydrophobic coatings can have other desirable properties, such as anti-icing and anti-fouling capabilities. These coatings can prevent the formation of ice on steel surfaces, reducing the risk of accidents and improving operational efficiency in cold environments. They can also inhibit the adhesion of marine organisms, reducing biofouling and improving the performance of steel surfaces in marine applications [9].

Overall, superhydrophobic coatings for steel offer a combination of water repellency, self-cleaning properties, corrosion resistance, and enhanced durability. These coatings have the potential to significantly improve the performance and lifespan of steel components in various industries, ranging from transportation and infrastructure to manufacturing and marine applications.

2.2 Superhydrophobic Coatings using Polyurethane:

In this study, using polyurethane and silica nanoparticles were used as the resin to coat the mild steel sample. The coating was created using a spin-coating technique and involved the use of polyurethane, SiO_2 nanoparticles, and hexadecyltrimethoxysilane [6].

Several techniques were employed to characterize the coated steel surface, including contact angle measurements, scanning electron microscopy, and Fourier transform infrared spectroscopy. Contact angle measurements provide information about the wettability of a surface, and in this case, the coated surface exhibited a water tilt angle of 4°±2° and a static contact angle of 165°±5°. These values indicate a superhydrophobic nature, meaning the surface repels water effectively.

Scanning electron microscopy was used to visualize the surface morphology and confirm the presence of the coating. Fourier transform infrared spectroscopy helps identify the chemical composition of the coating by analyzing its vibrational modes.

The study also conducted various tests to evaluate the performance and stability of the coating. Chemical stability tests assessed the resistance of the coating against different chemicals, while thermal stability tests examined its behavior under high temperatures. Mechanical stability tests evaluated the durability of the coating against mechanical stress.

Droplet dynamic studies were conducted to understand the behavior of droplets on the coated surface. The coating exhibited excellent self-cleaning properties, meaning that water droplets could effectively remove dirt and debris from the surface. Additionally, the coating demonstrated anti-fogging properties, preventing the formation of fog on the steel surface. Furthermore, the coated steel surfaces showed anti-corrosion properties, making them suitable for industrial applications where corrosion resistance is important.

Coatings that are superhydrophobic can become hydrophobic by adding organic functional groups like $-CH_2$, $-CH_3$, and $-CF_3$. These functional groups are present in a number of polymers, including polystyrene, polymethyl methacrylate, polydimethylsiloxane, and polypropylene, which have been used to make superhydrophobic coatings. Polyurethane is a flexible polymer that may be used for a variety of products, from medical equipment and cushions to seats and paints. It is noted for its mechanical strength, solvent resistance, thermal stability, and chemical resistance. In multiple investigations, researchers created superhydrophobic polyurethane coatings on metallic substrates.

For instance, West et al. [38] used a two-step plasma-fluoroalkyl treatment using polyurethane as the base material to create a superhydrophobic coating on low carbon steel. Using suspension flame spraying, Chen et al. [39] created superhydrophobic polyurethane and nano-alumina coatings on aluminum substrates. Through the sol-gel method, Yousefi et al. [40] created a polyurethane silica nanoparticle composite superhydrophobic coating on stainless steel wire mesh. Yang et al. created a fluorine-containing acrylic polyurethane coating for steel using the spin-coating method. Superhydrophobic polyurethane/MoS2 nanocomposite coatings were created by Tang et al. using a spray-coating process on steel, glass, cloth, and paper.

However, there have not been many in-depth studies of steel's superhydrophobic polyurethane coatings' capacity to resist corrosion as well as its chemical, thermal, and mechanical stability. The resultant superhydrophobic samples are put through arduous testing in severe environments, such as mechanical shocks, exposure to highly corrosive chemicals, and high temperatures, to determine their practical usefulness.

2.2.1 Results:

The discussion of the prepared steel samples' wettability comes first. The materials' surface morphology and FTIR spectra are next looked at. Data on the coatings' chemical, thermal, and mechanical stabilities are given. The results of the experiments on floating, bending, sand fall, and self-cleaning are then described. Data on droplet dynamics and anti-corrosion characteristics are also supplied.

Both uncoated and coated steel surfaces' wettability behavior was assessed using the contact angle measuring technique. SEM pictures of the coated and uncoated steel samples are shown in Figure 2, together with the corresponding contact angles. An uncoated steel surface with a static water contact angle of 47°2° demonstrates hydrophilic characteristics. The coated sample, however, exhibits outstanding water repellency after being coated with a superhydrophobic solution, showing a water contact angle (WCA) of 1655° and a tilt angle of 4°2°. The coated sample's SEM photos reveal microstructures, which most likely developed as a result of SiO2 nanoparticle aggregation within the polyurethane matrix. The existence of a low surface energy substance is shown by the rise in water's static contact angle upon coating [6].

In summary, this study focuses on the development and characterization of a polyurethane-based superhydrophobic coating on steel. It explores the coating's stability under various challenging conditions and investigates its water droplet behavior, self-cleaning properties, resistance to fogging, and ability to inhibit corrosion.

In this study, a superhydrophobic polyurethane-based coating was successfully developed on a steel surface using silica nanoparticles and

hexadecyltrimethoxysilane through a spin-coating technique. The coated steel sample exhibited a static water contact angle (WCA) of 165°±2° and a sliding angle of 4°±2°, indicating excellent water repellency. Analysis using scanning electron microscopy (SEM) revealed the presence of microstructures on the coated sample, while Fourier transform infrared spectroscopy (FTIR) confirmed the existence of functional groups such as -SiO- and -CH2-. Investigation of droplet dynamics on the coated steel surface demonstrated varied behaviors including bouncing, pinning, and splashing at different impact velocities.

The wettability of the coating was found to be resistant to mechanical disturbances caused by high-speed water jets, bending, and sand abrasion tests. Although the prepared coated samples corroded in highly acidic and alkaline media within a few hours, the wettability of the coating remained unaffected even after 40 days, indicating excellent chemical stability. Additionally, the coating demonstrated thermal stability up to 230°C.

Moreover, the prepared coated steel surface exhibited outstanding self-cleaning, anti-fogging, and anti-corrosion properties, making it highly suitable for numerous industrial applications.

2.3 Optically transparent nanoparticle composite coatings:

The development of hydrophobic SiO2 or photocatalytic TiO2 nanoparticle-based anti-soiling coatings. In order to reduce the surface area in contact with dirt particles while retaining optical performance, the coatings strive to produce nanoscale surface features and increase surface roughness. Two configurations are investigated: one based on assemblies of unstructured nanoparticles of various sizes and the other based on silica particles with surface nano-features and agglomerated particle structure. Fluorocarbons are functionalized in both forms to add water resistance [5].

The primary pollutants in desert regions, according to the study, are sand and dust particles. The adhesion force and energy necessary to remove silica-based contaminants from the nanostructured surface are measured using atomic force microscopy (AFM). Testing with falling sand and measurements of UV-visible transmission before and after soiling are used to assess how efficient the anti-

soiling is. Coated and uncoated mirror samples are subjected to field testing in a CSP facility to determine the daily deterioration rate of the coatings. The created coatings have promising anti-soiling capabilities, are adaptable to surfaces other than glass, and may be retrofitted and refinished on the spot.

2.4 Nanoparticle Assemblies with Bimodal Size Distribution

Using assemblies of unstructured nanoparticles with a bimodal size distribution is another method for developing coatings with multi-scale characteristics. The particles, which have diameters between 80 and 35 nm, are seen in the SEM. AFM pictures of the coated glass samples are shown, demonstrating surface features of various heights created by the aggregation of particles of various sizes. The bigger particles disperse over the surface with a separation distance of a few micrometers, whilst the smaller particles form densely packed and homogeneous coatings. With a multi-height design, the assemblies of particles with a bimodal size distribution produce more noticeable surface characteristic. The bigger features are spaced apart by about 2-3 m, and the features have heights of around 150-250 nm. The nanostructured particle assemblies from the first coating method, on the other hand, produce surface characteristics with a more uniform height of 60–80 nm. Fewer surface asperities are expected to come into contact with dust particles when a multi-height arrangement is designed, lowering the adhesion force between the dust and the coated surface. This arrangement intends to provide anti-soiling qualities for soil particles with a broad size distribution while maintaining good optical performance. Sub-micrometer soil particle adhesion force is reduced by the smaller-sized surface characteristics.

On samples of solar glass, soil tests were performed as per the prescribed protocol. Due to the antireflective qualities of the nanostructured coating, the coated solar glass displays transmittance values up to 2% greater than the untreated glass for wavelengths below 800 nm. After the soil test, the average transmittance values of the coated glass for wavelengths below 700 nm were up to 1% higher than the uncoated glass' pre-test values and more than 20% higher than the uncoated glass' post-test values. The coated glass measurement data show a standard variation of 0.5% or less. Comparatively, both prior to and

during the falling sand test, the transmittance values of the coating based on unstructured nanoparticle assemblies with a bimodal size distribution were around 2-3% higher than the comparable values of the coating based on nanostructured particles. A comparison plot of the average transmittance values of the two coating formulations before and after the sand falling test clearly shows that the coating based on particles with a nanostructured surface exhibits a more pronounced decrease in transmittance (difference in values before and after the sand test) for wavelengths below 700 nm. The second coating formulation, which is based on unstructured nanoparticle assemblies, also has anti-reflective qualities and is distinguished by a noticeably lower standard deviation in transmittance values.

Sand and dust repellency of samples of solar glass treated with nanostructured anti-soiling coatings was assessed. Using an AFM probe and a silica sphere, the adhesion force between the particles and the coated surface was modelled. The outcomes demonstrated that a 15-micrometer silica sphere could be removed from the coated solar glass surface with much less adhesion force and energy than from the uncoated surface. After being put through a falling sand test, the coated glass showed roughly 20% greater UV-vis transmittance values than the untreated glass. These results show that the created coatings may be scaled up and used on current solar installations, lowering maintenance costs and increasing energy efficiency and dependability. Field tests on coated solar mirrors showed a 17-39% reduction in soiling rates compared to uncoated mirrors.

2.5 Superhydrophobic Coatings in Steel:

Thanks to its great mechanical qualities, resistance to corrosion, and aesthetic appeal, stainless steel is a material that is utilized in a variety of applications. The hydrophilic nature of stainless-steel surfaces may be changed in this work to generate superhydrophilic, superhydrophobic, or superliquiphobic features, which might potentially further improve these properties. Hierarchical roughness and surface chemistry are combined to produce these useful surfaces. To achieve the necessary roughness, a variety of techniques including sandblasting, chemical etching, and nanocomposite coatings are used. Surface

chemistry is regulated by the use of methylchlorosilane, nanoparticles in methylphenyl silicone, and fluorosilane treatment [3].

This all-encompassing strategy enables direct comparisons between various paths. The resultant processes produce stainless steel surfaces with a 155° hexadecane contact angle and a 7–10° tilt angle. The report also discusses coating methods based on condensation reactions and rust-avoidance tactics.

The study also reveals the increased qualities on stainless steel 304 L acquired by these surface alterations, such as self-cleaning behavior, anti-icing behavior, better wear resistance, and improved bending resistance. Additionally, stainless steel 430, which is known to be more susceptible to corrosion than stainless steel 304 L, is used to illustrate the transferability of the treatments and the corrosion resistance conferred by superliquiphobicity.

Our goal in this work is to produce stainless steel 304 L with superhydrophilicity, superhydrophobicity, and superliquiphobicity. We use a variety of techniques, including as sandblasting, chemical etching, and nanocomposite coatings [3], to achieve the necessary surface roughness. According to sources, methyl chlorosilane, nanoparticles in methylphenyl silicone, and fluor silane are used in coatings to achieve super hydrophobicity and super liquiphobicity. These paths offer competing methods for introducing superliquiphilicity or superliquiphobicity, and their varied degrees of effectiveness provide information on how to change surface roughness and coating methods.

The characterized surfaces are evaluated based on contact angle and tilt angle measurements. Furthermore, their performance is analyzed in terms of self-cleaning and anti-icing behaviors, as well as durability through wear resistance and bending tests. The procedures used to create different wetting regimes on stainless steel 304 L are then applied to verify their effectiveness on stainless steel 430. Finally, stainless steel 430, which is known to be less corrosion resistant than stainless steel 304 L, is used to assess the corrosion resistance imparted by the superliquiphobic surface modification. For the initial set of tests, SS 304 L, a commonly utilized stainless steel, was chosen. The properties of the

unmodified surface were evaluated, specifically examining self-cleaning and anti-icing properties. Subsequently, we conducted tests to assess the durability of the nanoparticle binder coatings, which serve as the sole method for achieving superliquiphobicity. These tests included a reciprocating wear test and a bending test.

2.6 EPD:

Because of the many ways in which the electrophoretic deposition (EPD) technology may be used to treat advanced ceramic materials and coatings, it has attracted a lot of attention from both the academic and industry communities. One of the main factors contributing to this increased interest is its adaptability, since it can be utilized with a variety of materials and their combinations, along with its affordability and straightforward equipment needs [4].

EPD has a long history, dating back to 1808 when the movement of clay particles in water induced by an electric field was observed by the Russian scientist Ruess. However, it was not until 1933 that EPD found its first practical application when the deposition of thoria particles on a platinum cathode was patented for use in electron tube applications.

Although the basic phenomena underlying EPD are well understood and have been extensively studied both theoretically and experimentally, the application of EPD to ceramics was initially explored by Hamaker [10] in the 1980s within the field of advanced ceramics. Despite the progress made, there is a consensus among the scientific community that further research and development efforts are needed to achieve a comprehensive and quantitative understanding of the fundamental mechanisms of EPD. This understanding would facilitate the optimization of working parameters, leading to broader utilization of EPD in materials processing.

Electrophoretic deposition (EPD) is a versatile colloidal process used in ceramic production, offering several advantages such as short formation time, simplicity of apparatus, and the ability to deposit coatings without the need for binder burnout. Unlike other shaping techniques, EPD can easily be modified to suit

specific applications, allowing deposition on various substrate shapes with minor changes in electrode design and positioning.

EPD involves the attraction and deposition of charged powder particles suspended or dispersed in a liquid medium onto a conductive substrate of opposite charge under the influence of a DC electric field. It is important to note that "electrodeposition" is a term that is sometimes used ambiguously to refer to either electroplating or electrophoretic deposition, although it commonly refers to the former [10].

The distinction between EPD and electrolytic deposition (ELD) lies in the suspension of particles in a solvent for EPD, while ELD is based on the solution of salts. EPD can occur in two modes: cathodic electrophoretic deposition, where positively charged particles are deposited on the cathode, and anodic electrophoretic deposition, where negatively charged particles are deposited on the anode. By modifying the surface charge of the particles, mode of deposition can be achieved.

Beyond the usual ceramic coatings that are wear-resistant and anti-oxidant, EPD has discovered a wide range of technical uses. Additionally, it is employed in the creation of bioactive coatings for medical implants as well as functional films for solid oxide fuel cells, composites, and microelectronic devices. EPD has also become popular for the nanoscale construction of sophisticated functional materials [11].

Control of stoichiometry in EPD deposits is determined by the stoichiometry of the powder used, and the charged particles do not lose their charge upon deposition. The driving force for EPD is the charge on the particles and their electrophoretic mobility in the solvent under the influence of the electric field. EPD has been successfully employed in various applications, including silica films, nanosized zeolite membranes, hydroxyapatite coatings for biomedical applications, luminescent materials, superconducting films, and more.

One limitation of EPD is its inability to use water as the liquid medium due to the evolution of hydrogen and oxygen gases at the electrodes. However, this

constraint is minor considering the availability of numerous non-aqueous solvents that can be used in the process.

2.6.1 Factors influencing EPD:

Charged particles dispersed in a liquid media are deposited onto an electrode by electrophoretic deposition (EPD) when an electric field is applied. Two sets of parameters—those pertaining to the suspension and those pertaining to the procedure itself—determine the features of the EPD process [10].

Both the charged particles and the free ions in the solution have an impact on the quantity of particles that are deposited during EPD. However, the contribution of free ions is often insignificant in organic suspensions. The rate of deposition is thought to be affected by the buildup of anionic and cationic charge at the electrodes during electrophoresis, however this influence is minimal in the early stages of deposition.

To link the quantity of deposited particles with various influencing factors, several equations have been presented. The deposit yield is correlated by Hamaker's equation with the electric field intensity, electrophoretic mobility, electrode surface area, and particle mass concentration in the suspension. The electrophoretic mobility is increased by Avgustinik's law, which is based on cylindrical, coaxial electrodes in terms of permittivity, zeta potential, and suspension viscosity.

Biesheuval and Verweij [37] developed a more complex model considering three distinct phases: the deposit phase, the suspension phase, and a phase with few or no solid particles. Their equation considers the movement of the boundary between the deposit and suspension phases over time.

Other equations, such as those proposed by Ishihara et al. and Chen and Liu, focus on the weight of charged particles deposited per unit area of the electrode during the initial period. These equations consider factors such as particle concentration, permittivity, zeta potential, viscosity, applied potential, distance between electrodes, and deposition time. Overall, the mass of deposited particles and the thickness of the films in EPD can be controlled by adjusting the suspension concentration, applied potential, and deposition time.

2.6.2 Parameters related to suspension in EPD:

Particle size, dielectric constant of the liquid, conductivity of the suspension, viscosity of the suspension, and zeta potential of particles are all critical factors that significantly impact the electrophoretic deposition (EPD) process. The size of particles has a direct influence on the efficiency of deposition and the potential for crack formation in the deposited film. To achieve successful deposition, the dielectric constant of the liquid must fall within a specific range. The conductivity of the suspension needs to be carefully balanced to ensure optimal particle motion and stability. In the suspension vehicle, viscosity, dielectric constant, and conductivity are key parameters to consider. Furthermore, the zeta potential of particles plays a crucial role in determining their surface charge and stability, which directly affects the deposition rate and the density of the resulting deposit [33]. By carefully controlling these factors, the EPD process can be optimized for improved outcomes.

2.7 Parameters related to Process:

2.7.1 Time:

Numerous academics have looked at how the electrophoretic deposition (EPD) process is impacted by the deposition time. Basu et al., Chen and Liu [34-35], and others have noted that when deposition time is lengthened or increased, the deposition rate declines. The rate of deposition is initially linear but slows down as the deposition time rises and finally approaches a plateau at very high deposition times. This behavior is anticipated in constant voltage EPD because an insulating layer of ceramic particles on the electrode surface causes the electric field, which affects the electrophoresis process, to weaken with time. As a result, even if there is no change in the potential difference between the electrodes, the electric field's efficacy is decreasing. However, during the initial period of EPD, there is typically a linear relationship between deposition mass and time.

Weight of deposited hydroxyapatite on Ti6Al4V

substrate versus applied voltage for different

deposition durations: (a) 30 s and (b) 120 s
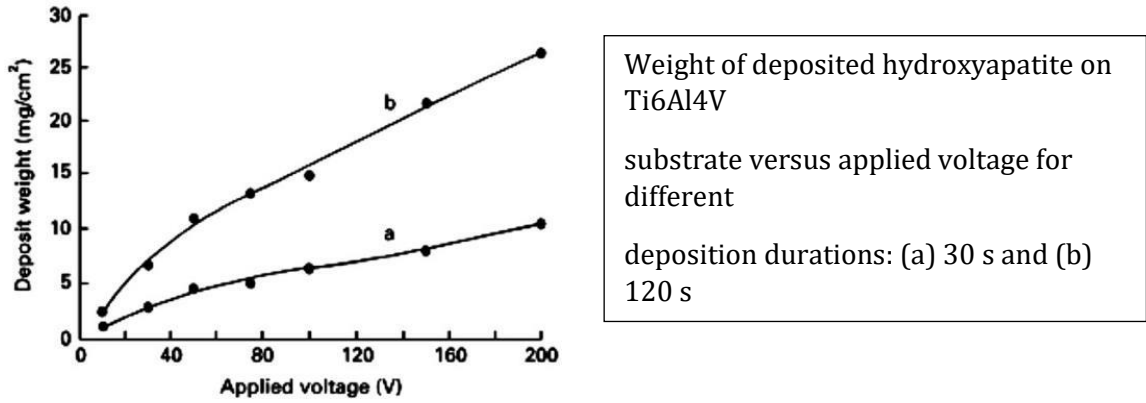
Figure 4, Applied voltage vs deposit weight graph.

2.7.2 Voltage:

The amount of deposit typically increases with an increase in the applied potential. While it is possible to achieve faster deposition rates by utilizing higher applied fields, it is important to consider the potential impact on deposit quality. Basu et al. [34] conducted experiments and observed that more uniform films were obtained at moderate applied fields ranging from 25 to 100 V/cm. However, when relatively higher applied fields exceeding 100 V/cm were employed, the film quality deteriorated. This phenomenon can be attributed to the kinetic nature of particulate film formation, where the rate at which particles accumulate influences their packing behavior during the coating process. When a higher applied field is used, turbulence in the suspension may occur, disrupting the orderly deposition of particles onto the substrate. Additionally, particles may move at an accelerated rate, preventing them from settling into their optimal positions to form a close-packed structure. Furthermore, in high-field situations, the lateral motion of particles deposited on the surface is restricted due to the increased pressure from the higher applied potential, affecting both the deposition rate and the structure of the deposit.

In the context of deposition from suspensions, the stability of the current density in the absence of any powder is an important consideration for achieving high-quality deposits. Negishi et al. [36] conducted studies on n-propanol solvent and observed that the current density was directly proportional to the applied voltage. However, as the applied voltage increased, the stability of the current

density tended to decrease. This unstable current density can have significant implications for the quality of the deposition morphology. The variations in current density stability serve as a valuable guideline for determining optimal deposition parameters, ensuring the formation of high-quality deposits through electrophoretic deposition (EPD). By carefully controlling the applied voltage within a stable range, it is possible to enhance the deposition process, resulting in improved deposit characteristics such as uniformity and morphology. Understanding the relationship between applied voltage and current density stability provides valuable insights for optimizing the EPD process and achieving desirable deposition outcomes.

2.7.3 Volume Fraction of Solids:

The concentration of solid particles in the suspension is a crucial factor, especially in multi-component electrophoretic deposition (EPD) systems. The volume fraction of solids plays a significant role in determining the deposition behavior of different particle species, even when they possess the same sign of surface charge. The deposition rates of these particles can vary depending on the volume fraction of solids in the suspension.

When the volume fraction of solids is high, the particles tend to deposit at a relatively equal rate. This is because the high concentration of particles facilitates their interaction with the electric field, leading to a more uniform deposition. In such cases, the particles are densely packed within the suspension, allowing for efficient deposition onto the substrate.

However, if the volume fraction of solids is low, the deposition rates of the particles can be influenced by their individual electrophoretic mobility. Electrophoretic mobility refers to the velocity at which a charged particle moves in an electric field. When the concentration of particles is low, the interactions between the particles become less frequent, and individual particle characteristics become more pronounced. Consequently, particles with higher electrophoretic mobility will tend to deposit at a faster rate compared to particles with lower mobility.

Therefore, the concentration of solid particles in the suspension is a critical parameter to consider in multi-component EPD systems. It can significantly affect the deposition behavior and rates of different particle species, ultimately influencing the composition and morphology of the deposited coating. Understanding the interplay between concentration, particle mobility, and deposition behavior is essential for controlling and optimizing the EPD process in multi-component systems [41].

2.7.4 Conductivity of Substrate:

Electrophoretic deposition (EPD), particularly in multi-component systems, is greatly influenced by the concentration of solid particles in the suspension. The quality of the produced green film and the deposition behavior can both be greatly influenced by the volume percentage of solids. According to research by Peng and Liu, sluggish deposition rates and uneven green film deposition were caused by the substrate electrode's poor conductivity, which was La0.9Sr0.1MnO3 (LSM). Chen and Liu [34] discovered a similar phenomenon when they employed LSM or LSM-YSZ composite pellets as substrates: the YSZ deposition rate was sluggish, and the resultant film had non-uniformity. This was attributable to the substrates' high resistance, which was brought on by the additional binder. However, when the pellets were fired to remove the binder, the conductivity of the substrates increased substantially, leading to the formation of high-quality green YSZ film.

The description above highlights how a variety of factors affect the kinetics of electrophoretic deposition and the deposit's quality. Therefore, during EPD, thorough management of each of these characteristics is required. As a result of their interdependence, several of these characteristics have an impact on one another. Particularly, suspension conditions are crucial in influencing the deposition's quality. In comparison to an unstable or agglomerated powder suspension, a well-dispersed and stable suspension is more likely to produce a superior deposition outcome. Zeta potential, which quantifies the potential difference between the particle surface and the shear layer plane created by the adsorbed ions, is one crucial metric associated with suspension stability and mobility. Better particle dispersion in the suspension is indicated by a greater

absolute zeta potential value. Since the ions in the suspension are what carry the majority of the current when an electric field is applied, the electrical conductivity of the suspension is also crucial to the EPD process. Due to the adsorption of H+ ions on particle surfaces, the zeta potential rises when the pH value drops from 7.5 to 4.5, increasing the electrostatic repulsion force. But a further pH falls from 4.5 to 2.0 results in a thinner double layer, decreasing the repulsive force and encouraging particle agglomeration. In the alkaline range, a similar process happens, but OH ions in the suspension are adsorbing instead. It is important to keep in mind that the absolute magnitude of the zeta potential in the alkaline range is often smaller than that in the acidic range. The electrical conductivity of the suspension is correlated with the ionic concentration, which also impacts the zeta potential. Increased agglomeration and the creation of bigger, less mobile agglomerates are both possible effects of high ionic concentration. Additionally, the number of free ions in the solution may act as the primary current carrier, decreasing the mobility of the particles during electrophoresis. Additionally, the dielectric constant of the suspending medium has a direct impact on the conductivity of the suspension, rising as the dielectric constant rises. Therefore, careful selection of suspension parameters is essential for preparing a suitable EPD suspension [41].

2.8 Melamine Formaldehyde: Our Solution.

Melamine formaldehyde (MF) is a highly durable and rigid thermosetting polymer that offers excellent properties and performance. As an amino resin, it possesses numerous advantages such as transparency, hardness, thermal stability, resistance to boiling, scratch resistance, abrasion resistance, flame retardancy, moisture resistance, and surface smoothness. These advantageous properties have led to extensive industrial applications of MF in various fields. Initially used as wood adhesives, MF resins are now utilized in flooring and decorative laminates, molding compounds, coatings, and adhesives. Their toughness and ease of manufacture make them valuable in a wide range of products [1].

The curing behavior and degree of crosslinking in MF resins determine their tailored properties, including mechanical, thermal, and electrical characteristics.

Once cured, MF polymers exhibit high hardness and resistance to temperature, chemicals, and hydrolysis, making them suitable for interior working surfaces. Proper curing is essential to ensure that MF resins possess sufficient mechanical strength and surface finishes. Insufficient curing can result in drawbacks such as reduced hardness, durability, brilliance, and resistance to hydrolysis and chemical agents, particularly evident in MF-impregnated papers.

The condensation reaction and resulting structure of MF resins vary significantly depending on reaction conditions such as molar ratios of reactants, pH, and reaction temperature profiles during resin preparation. Therefore, studying the curing process of MF resins holds immense importance.

Numerous research groups have investigated the reaction between melamine and formaldehyde [2]. The addition reaction between melamine and formaldehyde has been studied using reversed-phase liquid chromatography, enabling the assignment and quantitative analysis of methylol melamines in the reaction mixtures. Structural studies of soluble MF resins have been conducted using 13C nuclear magnetic resonance (NMR), providing insights into the reactions and structures of these resins. Additionally, the elucidation of the structure of melamine-formaldehyde-polyvinylpyrrolidone has been reported using 1H NMR and 13C NMR, identifying the methylol, methylene, and methylene ether structures. The kinetics of the addition reaction between melamine and formaldehyde in the aqueous phase during the initial stage of resin formation have also been investigated.

The formation of MF resin involves two stages: methylolation and condensation. The initial investigations into these reactions were conducted by Okano and Ogata. In the first stage, melamine reacts with formaldehyde, resulting in the production of a series of nine distinct methylol melamines, starting from monohexamethylol melamine. In the second stage, condensation reactions occur, leading to the formation of various oligomers containing methylene and methylene ether bridges. The ratio of these two types of bridges during the condensation reaction depends on the pH of the reaction medium. At relatively low pH values (7-8), methylene bridges are dominant, while at high pH values above 9, ether bridges are favored [12].

Bauer and Dickie [20] used infrared spectroscopy (IR) to examine the cure chemistry and network development of two acrylic copolymer resins crosslinked with several MF-based crosslinkers. This study considers variables including resin composition, melamine type, concentration, cure temperature, and cure time to give insights into the amount of interaction between the hydroxy and carboxy groups of the acrylic copolymer and the methylol group of the MF crosslinker. A statistical model was used to calculate the effective crosslink density using the data that were gathered.

David [43] studied the chemistry of melamine crosslinking, network creation, and coating degradation. For completely alkylated melamine, the author suggested a particular acid-catalyzed process, while for partly alkylated melamine, a more generic acid-catalyzed mechanism. Another study employed FTIR analysis to examine the crosslinking reaction between a highly substituted methylated MF resin and a hydroxyl functional polyester. This study showed that ether crosslinks develop in the early phases of curing before all hydroxyl groups are consumed, and ether intermediates are used to generate methylene bridges.

Using FT-Raman spectroscopy in conjunction with 13C NMR, liquid chromatography, and other techniques, it has been possible to better understand how methylolation and the production of ether-methylene bridges occur in MF resin. Additionally, the crosslinking of polyurethane dispersions with MF resin, leading to co-condensation reactions, has been studied by Mequanint and Sanderson.

2.9 Reaction Studies and Mechanism:

The reaction mechanisms and pathways involved in the crosslinking of MF resins are complex, and the chemical characterization of cured resins is challenging due to their insolubility. While the empirical understanding of the curing processes of MF resins is well-established, there is still a need for more detailed methods to gain a deeper understanding of the chemical reactions occurring during condensation.

Previous research mainly focused on elucidating the methylolmelamines and their reaction pathways, with only a few attempts made to investigate the

crosslinking reaction mechanism. Some studies have explained the crosslinking mechanism of MF resin in water, leading to the formation of ether bridges. The crosslinking mechanisms of fully alkylated and partially alkylated MF resins with catalysts have also been explored. Gas chromatography analysis of the volatiles formed during the crosslinking reaction provided insights into the catalyzing mechanisms.

Researchers have studied the initial methylolation and subsequent thermally induced condensation reactions, which involve the formation of ether links that readily decompose into methylene links above a certain temperature. This reaction sequence is accompanied by demethylolation, resulting in the release of free amine. However, a complete reaction mechanism for MF resin is still under investigation [24].

The reversible demethylolation occurring during the cure reaction of MF resin has been reported with and without the presence of a catalyst, but the temperature range at which demethylolation dominates over the crosslinking reaction, and vice versa, for a pure non-alkylated MF resin, remains unclear [25].

Although numerous research studies have been conducted on the curing of MF resin, there is a need for clarity in the reaction mechanism. Thermal and spectroscopic tools can provide valuable insights into the reaction stages, temperatures, and reaction routes of MF resin. The authors of this paper propose to elucidate the reaction mechanism by using techniques such as FTIR, differential scanning calorimetry (DSC), and thermal gravimetric analysis (TGA). They aim to clarify the temperature at which each reaction step occurs for a non-alkylated MF resin without a catalyst, as supported by FTIR analysis, and subsequently propose a comprehensive reaction mechanism. The paper focuses on correlating DSC, FTIR, and TGA thermograms of thermally cured MF resin and provides details on the synthesis and characterization of the resin. The novelty of the study lies in the correlation of DSC and TGA thermograms, which brings new insights into the curing process of MF resin [2].

2.9.1 Step 1: Methyloation

The methylolation step in the formation of MF resin involves the direct reaction between melamine and formaldehyde, resulting in the formation of methylolamine. This step is well-studied and can be represented by the following reaction:

Melamine + Formaldehyde → Methylolamine

During this step, the formaldehyde molecule reacts with the amino groups of melamine, leading to the attachment of methylol (CH_2OH) groups to the melamine molecule. The reaction can occur multiple times, resulting in the formation of a series of methylolmelamines with different degrees of methylolation.

The methylolation reaction is crucial in the initial stage of MF resin formation, and the extent of methylolation affects the subsequent condensation reactions and the properties of the cured resin. Understanding and controlling the methylolation step is important for tailoring the desired properties of the final MF resin product.
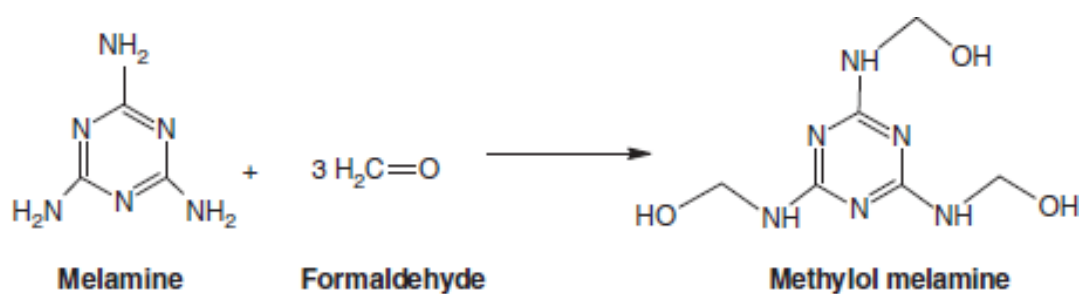
Figure 5, Reaction between melamine and formaldehyde.

2.9.2 Step 2: Condensation

During the condensation step, which is a complex process, multiple reactions occur that result in the formation of intermediate compounds containing ether

linkages. These ether linkages are later converted into methylene linkages through the elimination of formaldehyde, as depicted in Scheme 1.

However, the authors propose the existence of an additional reaction pathway that contributes to the formation of methylene bridges in the final cured product. This alternative pathway involves the reaction between the methylolamine generated in the methylolation reaction and melamine.

In simpler terms, while the conventional understanding suggests that formaldehyde elimination transforms ether linkages into methylene linkages, we believe that the reaction between methylolamine and melamine also plays a role in creating the methylene bridges in the cured MF resin.

This proposed reaction pathway warrants further investigation to determine its significance in the overall curing process and the resulting properties of the cured MF resin. Experimental studies and analysis would be necessary to confirm the existence and impact of this suggested reaction between methylolamine and melamine in the formation of methylene bridges.

Gaining a comprehensive understanding of the various reaction mechanisms involved in the formation and curing of MF resins is crucial for optimizing their properties and tailoring them to specific applications. Continued research in this area can provide valuable insights into the chemistry and behavior of MF resins during the curing process.

The reaction was carried out 140-160 degree Celsius. Another important point worth noting is that the reaction is reversible so needs attention for appropriate results.
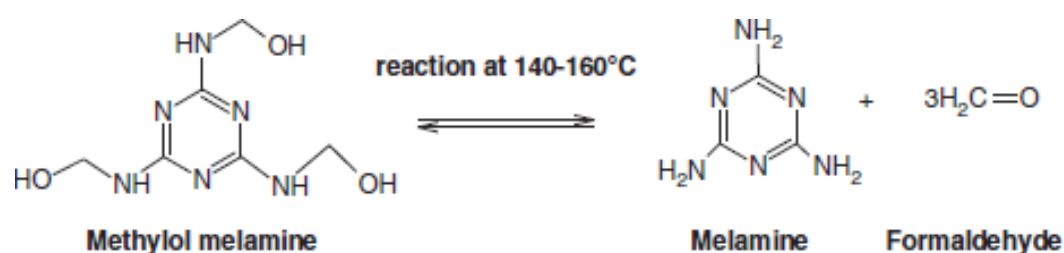
Methylol melamine   reaction at 140-160°C   Melamine   Formaldehyde

2.9.2.1   Overall Reaction:
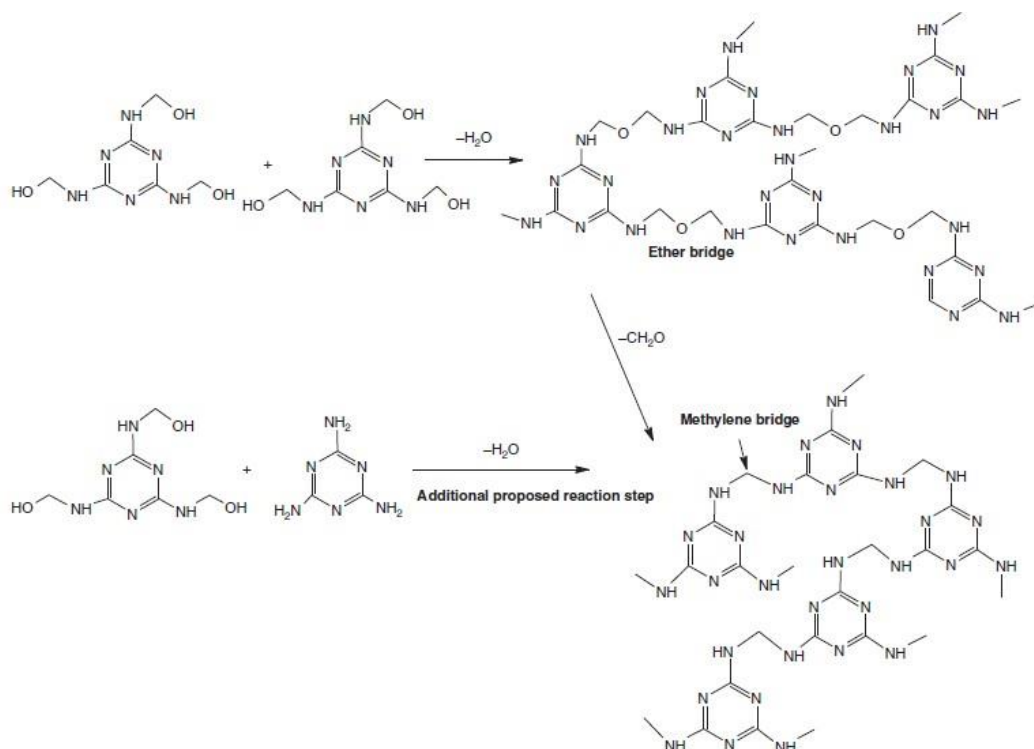
Scheme 1 Reaction mechanism of thermal curing of MF resin.

Figure 7, Overall reaction.

The curing mechanism of MF resin has been investigated through thermal and spectroscopic studies. The differential scanning calorimetry (DSC) thermogram displayed two distinct exothermic peaks, indicating a two-stage curing process. Further analysis using Fourier-transform infrared spectroscopy (FTIR) at the temperatures corresponding to these exothermic peaks provided insights into the two-stage crosslinking reaction mechanism.

The first step of thermal curing, occurring in the temperature range of 140-160°C, involves the reverse reaction of methylol groups to melamine. The second step, taking place at temperatures above 160°C, corresponds to the crosslinking reaction. By combining the findings from DSC and FTIR studies, a plausible reaction pathway for the thermal curing process was established.

To describe the weight loss that occurs throughout the curing process, a thermogravimetric analysis (TGA) was carried out. The TGA data unmistakably demonstrated four sequential mass losses in the 50–600°C temperature range,

which was consistent with the findings from the DSC thermogram. The weight loss was caused by the evaporation of water and formaldehyde, according to the link between DSC and TGA. The DSC-TGA thermogram, which showed two peaks in the same temperature range, also corroborated the two-step curing method. The weight loss caused by the removal of formaldehyde during the MF resin's reverse reaction was represented by the first peak at 160°C, while the water elimination during the condensation reaction was shown by the second peak [2].

It is important to note that the methylene bridges formed during the curing process remain stable up to 350°C, while the thermal degradation of the triazine ring begins at 400°C.

Overall, the combination of DSC, FTIR, and TGA studies provided valuable insights into the curing mechanism of MF resin, elucidating the temperature ranges, reaction steps, and weight loss patterns associated with the curing process. Understanding these aspects is essential for optimizing the properties and performance of MF resins in various applications.

2.10 Study of Melamine Formaldehyde in coating applications:

The use of nanomaterials in melamine-formaldehyde resin (MFR) has gained global attention due to their exceptional properties such as high effectiveness, thermal stability, fire retardancy, excellent physical-mechanical properties, good technological properties, and biocompatibility. This review aims to survey the existing literature on the utilization of nanomaterials to enhance the performance of MFR [1].

Because of its exceptional adhesive qualities and water resistance, MFR adhesives are often used. The performance of polymer composites may be greatly enhanced by including nanotechnology; this strategy has been extended to improve the characteristics of wood composites utilizing MFR. MFR is also often utilized as a thermoset resin in coating applications. Advanced MFR-based polymers for industrial coatings can be created using nanotechnology, improving their performance and characteristics. The development of nanomaterials recently and their influence on enhancing the functionality of MFR adhesives are highlighted. The decrease of free formaldehyde emissions, as well as mechanical

characteristics, thermal stability, and fire retardancy, are all thoroughly researched and addressed. The incorporation of nanoparticles into liquid MFR adhesives has the potential to significantly reduce environmental and health hazards.

2.11 Advantages and Disadvantages of Melamine Formaldehyde Resin:

Melamine-formaldehyde resin (MFR) is a widely used amino resin that is prepared by reacting melamine with aqueous formaldehyde. This resin has gained popularity as a thermosetting polymer due to its numerous advantages. MFR adhesives, which are nitrogen-rich amino resins with a stable triazine ring structure, offer several beneficial properties, making them suitable for a wide range of industrial applications.

One of the key advantages of MFR is its thermal stability, which allows it to withstand high temperatures without degrading. It also exhibits excellent fire retardancy, making it a preferred choice for applications where fire resistance is important. Additionally, MFR has low thermal conductivity, which contributes to its insulation properties. These characteristics make MFR suitable for use in construction and automotive industries.

MFR adhesives are known for their low emission levels, which is advantageous in terms of environmental and health considerations. They also offer good moisture resistance and are highly durable, ensuring long-lasting performance. MFR coatings provide a transparent finish and are resistant to the formation of molten drops, making them suitable for various applications [45].

The versatility of MFR extends to its applications in the wood industry. It is widely used as a wood adhesive for flooring and the production of laminates. MFR is also utilized in molding compounds, textile finishes, coatings, and adhesives. Its toughness and ease of manufacture make it a popular choice for a broad range of products [44].

Recent research has focused on enhancing the properties of MFR adhesives. For instance, the addition of Polyvinyl Alcohol (PVA) and nano-silica modified with 3-aminopropyltriethoxysilane (KH-550) has been shown to improve the

toughness, fire retardancy, thermal stability, and mechanical properties of MFR. These advancements open up new possibilities for MFR in various applications.

In summary, melamine-formaldehyde resin offers a host of advantages, including excellent temperature resistance, fire retardancy, moisture resistance, and mechanical durability. Its unique surface properties and low emission levels make it suitable for diverse industrial applications, ranging from decorative laminates to coatings and panel production. Ongoing research efforts aim to further enhance the properties and expand the utility of MFR in different fields.

2.12 Nanoparticles in Melamine Formaldehyde Resin:

The incorporation of nanoparticles into melamine-formaldehyde resin (MFR) offers a practical approach to developing multifunctional MFR nanocomposites with improved properties. Polymer nanocomposites, which consist of a polymer matrix and nanoscale fillers, have gained significant interest due to their remarkable enhancements in mechanical and physical performance. Nanotechnology has opened up new possibilities for creating materials with excellent properties and improved products for various industrial fields.

While there have been extensive studies on nanocomposites, there is limited research specifically focused on evaluating nanoparticles in the adhesives industry. However, in the wood composite industry, where adhesive bonding quality plays a crucial role in the properties and performance of wood-based composite products, the evaluation of nanoparticles becomes significant.

Even at modest addition levels, nanomaterials can have a significant impact on the final characteristics of MFR nanocomposites, such as their mechanical characteristics, curing behavior, formaldehyde emission, and flame retardancy. Novel materials with improved qualities may be produced by incorporating nanoparticles into the MFR matrix, opening up potential uses in a variety of industrial settings.

The properties of MFR nanocomposites can be strengthened by adding various nanofillers, such as clay minerals (such as montmorillonite nano clay, silica, and kaolinite), oxides (such as TiO_2, SiO_2, and alumina oxide), carbon-based

nanomaterials (such as carbon nanotubes, graphite, and cellulose nanofiber), and metals and metal alloys (such as Al, Fe). When making ornamental papers, these nanofillers help to increase the adhesive's distribution across the paper's surface and core. The dispersion of nanoparticles in the adhesive matrix reduces stress concentration, improves mechanical performance, and maintains or increases flexibility. nanoparticles can improve the physio-mechanical performance of the adhesives employed.

For altering MFR adhesives, researchers have investigated a number of additives, including polyvinyl alcohol (PVA) and benzoguanamine (BG). The structure, tensile strength, anti-fouling capabilities, heat stability, and char structure and morphology of MFR laminates have all been proven to be improved by these modifiers. The structural alterations in the modified MFR adhesives have been verified by spectroscopic investigations, including FTIR and 13C NMR.

In summary, the incorporation of nanoparticles into MFR offers the potential to develop MFR nanocomposites with enhanced properties. These nanocomposites can exhibit improved mechanical properties, curing behavior, formaldehyde emission, flame retardancy, and more. The selection and dispersion of nanofillers play a crucial role in achieving the desired properties. Further research and development in this area will contribute to the advancement of MFR-based nanocomposites for various industrial applications.

Common nanomaterials and their performance of MFR polymers.

Type of nanomaterials		Properties
Mineral nanoparticles	Clay	Low cost, mechanical reinforcement, flame retardant, thermal resistance,
	Na-montmorillonite (Na-(MMT))	Reduce formaldehyde emissions, improvement of bonding strength
Bio-based additive	Carbon nanotubes (MWCNT)	Mechanical strength,
	Cellulose nanofiber	Thermal conductivity,
	Cellulose nanocrystals (NCC)	Reduce formaldehyde emissions, improvement of bonding strength accelerated of
	Micro fibrillated cellulose (MFC)	curing time
	Hemp Flour	
Metal-based nanoparticles	Ag	Anitimicrobial properties
	Ni	Enhanced electrochemical/capacitive performance
Oxides nanoparticles	TiO_2	Mechanical and thermal reinforcement,
	SiO_2	Reduce formaldehyde emissions
	Alumina	Fire retardancy

Figure 8, Comparing nanomaterials.

Reference [1]: Dorieh, A., Farajollah Pour, M., Ghafari Movahed, S., Pizzi, A., Pouresmaeel Selakjani, P., Valizadeh Kiamahalleh, M., Hatefnia, H., Shahavi, M.H. and Aghaei, R. (2022). A review of recent progress in melamine-formaldehyde resin-based nanocomposites as

coating materials. *Progress in Organic Coatings*, 165, p.106768. https://doi.org/10.1016/j.porgcoat.2022.106768.

2.13 Formaldehyde Emissions:

Formaldehyde emission (FE) is a significant concern in the performance of melamine-formaldehyde resin (MFR) and wood-based composites. High levels of formaldehyde emissions can have negative effects on human health and the environment. However, modifying MFR nanocomposites can help control and reduce formaldehyde emissions.

Studies have shown that incorporating nanoparticles into MFR can effectively reduce formaldehyde emissions in wood-based panels. For example, the addition of nano-TiO2 and montmorillonite (MMT) nanoparticles to melamine-urea-formaldehyde (MUF) resin coatings on particleboards resulted in formaldehyde emissions 22-36% lower than other wood-based panels. The presence of nanoparticles enhanced the mechanical and physical properties of the coated boards while reducing formaldehyde emissions.

Polyvinyl acetate (PVC) has also been investigated as an additive to decrease formaldehyde emissions in MFR adhesives. The addition of PVC as a replacement for MFR adhesive led to a decrease in formaldehyde emissions, with emissions falling below the E1 class limit when PVC content reached approximately 30%.

Caprolactam has been used as an impregnating agent with MFR to reduce formaldehyde emissions. Caprolactam not only decreased formaldehyde emissions from MFR but also acted as a formaldehyde scavenger, capturing formaldehyde released from the resin.

The introduction of hemp flour (HF) as a filler into MUF adhesive has shown promise in reducing formaldehyde emissions. HF, with its high protein content, acted as a formaldehyde catcher and significantly reduced formaldehyde emissions. The content of added HF also influenced the mechanical properties, such as internal bond strength and modulus of elasticity, of the prepared boards.

In the case of wood-based products with melamine-decorative papers, the use of nano fillers, such as nano-TiO2 and nano-MMT, at varying loading levels (0.5% and 1%) resulted in decreased formaldehyde emissions. Both types of nano

fillers exhibited similar reductions in formaldehyde emissions, with higher loading levels contributing to slightly lower emissions compared to the control samples.

Overall, the incorporation of nanoparticles and additives, such as PVC, caprolactam, and hemp flour, into MFR has shown promise in reducing formaldehyde emissions from wood-based composites. These modifications not only enhance the properties of the composites but also contribute to improved environmental and human health outcomes [44-45].

<div align="right">

CHAPTER 3

</div>

<div align="center">

METHODOLOGY

</div>

3.1 Introduction

This chapter covers the synthesis of melamine formaldehyde using various methods and selecting the best method for resin synthesis. It also includes the integration of silica nanoparticles with melamine formaldehyde to form a composite.

3.2 Synthesis of MF

Resin was synthesized using two methods, by direct combination of melamine powder with formaldehyde and by using normalized formaldehyde solution in a melamine solution. The materials used, equipment and apparatus are also discussed in this chapter. [2]

3.2.1 Chemicals and materials used:

- Melamine
- Formaldehyde
- Dimethyl sulfoxide (DMSO)
- Tetrahydrofuran (THF)
- Sodium hydroxide (NaOH)
- Hydrochloric acid (HCL)
- Acetone
- Ethanol
- Mild Steel

Acetone and Ethanol were used to clean the apparatus and equipment. HCL and NaOH were used to maintain the pH.

3.2.2 Apparatus Used:

For the synthesis, the following apparatus was used.

- Clamping stand
- Hot plate
- Round bottom flask
- Thermometer
- Beakers
- Spatula
- Magnetic stirrer
- Mortar and Pestle
- Condenser tube
- Petri dishes
- Drying oven
- Water pump
- Weight balance
- Pipette
- Micropipette

3.2.3 Apparatus

A vertical condenser was used to condense the evaporating formaldehyde because the temperature was high enough to agitate the solution.
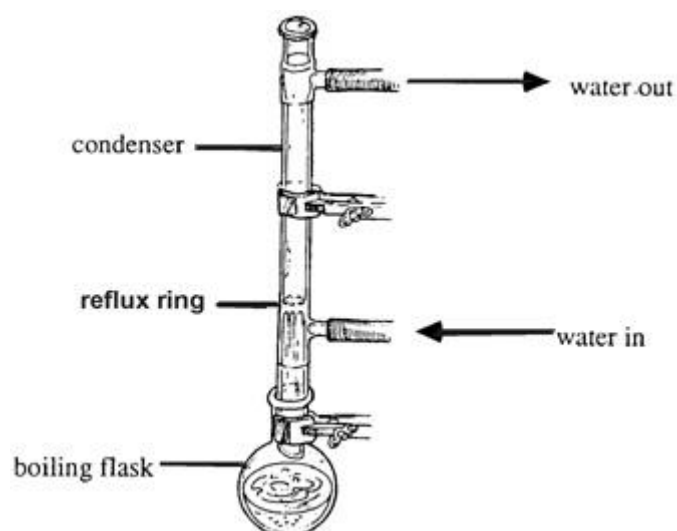

Figure 9, Apparatus of vertical condenser.

3.2.4 Procedure

Melamine Formaldehyde Resin was prepared following various approaches to arrive at the optimal result. Melamine powder and formaldehyde 37% in aqueous methanol solution were purchased from sigma Aldrich. Other organic solvents such as DMSO, THF, Acetone, Ethanol were also used in experimentation.

For preparation of resin a 1N NaOH solution and conc. HCl solution was also prepared.

Resin was synthesized using two methods and the methods were compared to select the best.

For approach A, melamine and formaldehyde were combined in a ratio of 1:3 and added to a condenser setup with temperature of 70-80 ° C was used. Once a clear solution was obtained, the pH was adjusted to 8-9 using 1N NaOH solution. The solution was allowed to sit under high temperature (80 Degrees Celsius), to cross-link and polymerize the resin. Solution was further vacuum dried in an oven to obtain the resin powder.

For approach B, melamine was dissolved in a solution of THF, and formaldehyde was adjusted using 1N NaOH to a pH of 8.5-9. The solutions were combined in a condenser setup and heated to 60 Degree Celsius to obtain a clear resin which was further air dried.

3.2.4.1   Treatment of MF Resin:

MF resin obtained from experiment A was further used as it was of highest purity (checked by FTIR). The resin powder was obtained by drying the resin in vacuum oven for a temperature of 50 Degrees Celsius for 12 hours.

3.2.4.2   Commination

The powder obtained had a crystalline form, which was later crushed manually, using mortar and pestle. Using this method, extremely fine powder is obtained. The use of mortar and pestle is necessary because a fine powder.

Figure 10, Powder grinding using mortar and pestle.

3.2.4.3   MF resin weighed:

A beaker was placed on the weight balance, and it was tared to zero. After this powder was added approximately to the weight of 2 grams.

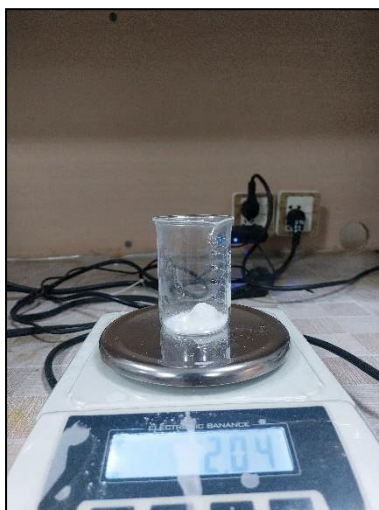*Figure 11, Weighing the powder.*

3.2.4.4   MF resin solution:

MF resin powder obtained was combined with organic solvents to check for their solubility, these solvents included, DMSO, Xylene, n-butanol, methanol, and De-ionized water.

The best result obtained was in DMSO, which gave complete solubility in a ratio of 1:5 of powder to solvent. So, for a 2 gram of MF powder 10 ml of DMSO was added.

After adding 2 gram of MF powder the weight balance was tared again. Then using a pipette 10ml of DMSO was added to powder. A magnetic stirrer was placed in the beaker and the beaker was placed on top of the hot plate. The temperature was set at 150 while the mixing was set at 1000 rpm. To make sure that DMSO was not evaporating and leaving the system, an aluminum foil was placed on top of the beaker as it can be seen in the picture.

Figure 12, Mixing MF powder with DMSO.

3.2.4.5   MF and Silica nanoparticles composite:

The silica nanoparticles were mixed with ethanol. Different composition of solutions of silica nanoparticles were created from 0.1 to 0.8 weight percentage against the total solution. [19]

3.2.4.6   Application:

The MF resin solution obtained was applied on a steel sample already prepared. The steel sample was grinded to emery paper number 1000, to obtain a clear surface, The sample was cleaned in ethanol and degreased using ethanol as well.
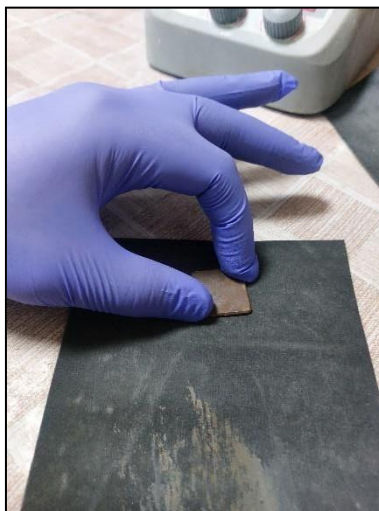
Figure 13, Cleaning sample using emery paper.

After the sample is thoroughly cleaned, the sample is attached to the EPD cell as shown in the following picture.

Figure 14, Sample attached to the EPD cell using screws.

3.2.4.7 Optimization

Using an EPD [4] cell, the sample was coated with the prepared resin solution. With the sample as cathode the solution containing resin powder was added to the cell, and various voltage values at varying intervals of time.

Using a tabulated data, optimal voltage and time was identified for coating thickness and uniformity. The voltage was varied between 30-90 V and the time was varied between 2-10 min.

Voltage/V	Time/min
30	2
30	4
30	6
30	8
30	10
45	2
45	4
45	6
45	8
45	10
60	2
60	4
60	6
60	8
60	10
75	2
75	4
75	6
75	8
75	10
90	2
90	4
90	6
90	8
90	10

Figure 15, Tabulated form of the variation of time and voltage.
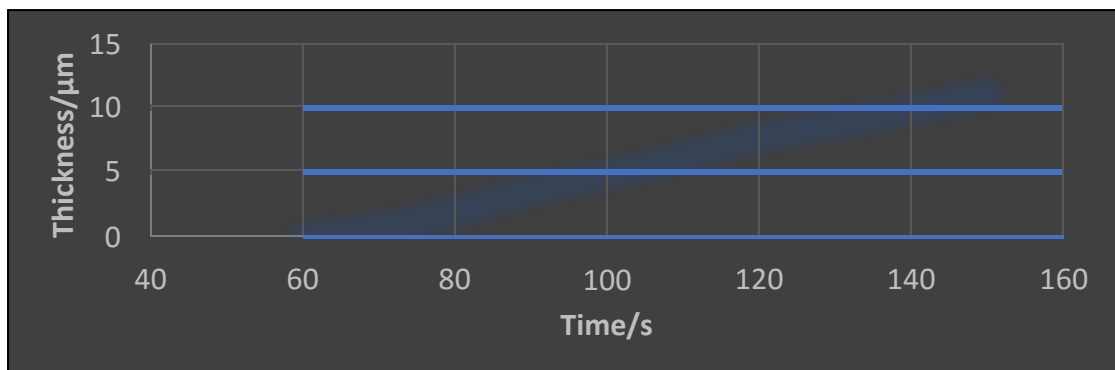
Keeping all other variables constant, the variations mentioned in the table were experimented. The best result was obtained at 60 V for 2 mins.

Figure 17, EPD cell connected to a DC supply with a voltage of 60.

MF resin was semi-cured on to mild steel by placing it in the oven at a temperature of approximately 150 degrees for about half an hour. The solution of ethanol and silica nanoparticles was mixed and placed in ultrasonicater for an hour at room temperature. The sample was then taken out and the solution of silica nanoparticles was drop casted on to the resin. After which the coating was fully cured at 150 degrees for 2 hours.

Figure 18, Drying oven set a temperature of 150 degrees.

The final coating can be seen in figure 19, the coating is transparent and superhydrophobic.

Figure 19, Final coating.

CHARACTERIZATION TECHNIQUES

4.1 Characterization techniques

4.1.1 FTIR:

Fourier Transform Infrared Spectroscopy (FTIR) is an analytical method widely used for assessing the chemical composition of materials by analyzing their interaction with infrared light. It provides detailed insights into the functional groups and molecular vibrations present in a sample, facilitating compound identification and bond analysis.
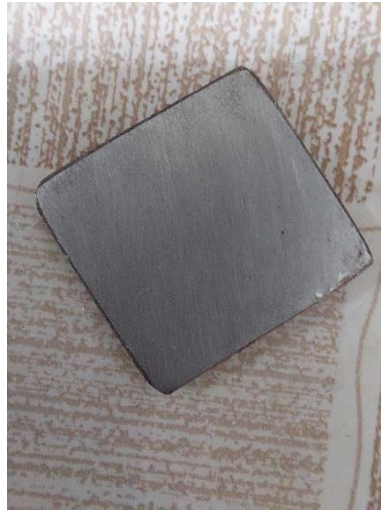
The premise behind FTIR spectroscopy is that molecules absorb infrared light at certain wavelengths that are distinctive of their molecular structure. Certain frequencies are absorbed when infrared light passes through a sample, resulting in a distinct absorption spectrum. The chemical composition of the sample can be established by comparing this spectrum to reference spectra or libraries.

The FTIR spectrum is commonly separated into many regions [14]:

Fingerprints Region (1500-400 cm^{-1}): This region has intricate patterns of molecular vibrations that provide information about the overall molecular structure and can help with compound identification.

Functional Group Region (4000-1500 cm^{-1}): Shows absorption bands associated with various functional groups, such as carbonyl (C=O) and hydroxyl (O-H).

Overtones and Combination Bands: Higher-energy regions including harmonics and combinations of fundamental vibrations, which provide information on the molecular structure. The following is the working mechanism of FTIR.

An empty sample compartment or a reference material is measured to establish a baseline spectrum. This allows for the removal of background noise and interferences.

The sample is placed in the sample compartment and an infrared light is sent through it. The ensuing contact with the sample results in an interferogram, which contains information about the material's absorption characteristics.

Fourier processing is used to the interferogram, which converts time-domain data into a frequency-domain spectrum. This process produces an infrared spectrum that depicts the sample's absorption peaks and intensities.

Specialized software is used to process and interpret the obtained spectrum. There are other ways, such as baseline correction, smoothing, and

To identify functional groups and chemicals present in the sample, the resulting infrared spectrum is compared to reference spectra or spectral libraries. Peaks and absorption bands in the spectrum correspond to distinct molecular vibrations, allowing the chemical makeup of the sample to be determined.

4.1.2 SEM

The resulting infrared spectrum is compared to reference spectra or spectral libraries to identify functional groups and chemicals present in the sample. Peaks and absorption bands in the spectrum correspond to distinct molecular vibrations, which aid in determining the chemical composition of the material.

SEM works based on electron-matter interactions. It scans the sample surface with a focused beam of high-energy electrons, generating signals that are recognized and processed to form an image.

Following is the working mechanism of SEM.

SEM generates a beam of electrons using a tungsten filament or a field emission source. To prevent electron scattering, the electron source is kept at a high vacuum.

A high voltage put between the electron source and the sample accelerates the emitted electrons. Typically, the accelerating voltage ranges from a few kilovolts to several tens of kilovolts.

Prior to imaging, the sample must be properly prepared. To improve conductivity and limit charging effects during imaging, the sample may be sliced, polished, and coated with a thin layer of conductive material (e.g., gold or carbon).

In a raster pattern, the concentrated electron beam is traversed across the sample surface. This is accomplished using electromagnetic scanning coils, which move the electron beam horizontally and vertically.

Interactions between the electron beam and the sample: When the electron beam interacts with the sample, numerous interactions occur, creating various signals:

Secondary Electrons (SE): Low-energy electrons emitted from the sample surface because of the primary electron beam's excitation. These electrons contain information about the topography of the sample.

Backscattered Electrons (BSE): Higher-energy electrons that scatter elastically, resulting in varying signal intensities depending on the atomic number of the material. Compositional and elemental contrast are provided by BSE signals.

X-rays: Primary electron interactions with sample atoms can result in the emission of distinctive X-rays. These X-rays are collected and analyzed to identify the sample's elemental composition.

Secondary electrons, backscattered electrons, and X-rays that are emitted are detected using proper detectors. Everhart-Thornley detectors for SE signals and solid-state detectors for BSE signals and X-rays are the most used detectors.

The detected signals are processed, amplified, and turned into electrical signals that describe the topography and composition of the sample's surface. These signals are utilized to generate high-resolution pictures of the sample in black and white or color.

4.1.3 EDS

X-ray Energy-Dispersive Spectroscopy (EDS) is a technique for identifying and analyzing the elemental composition of materials that is used in conjunction with

scanning electron microscopy (SEM). EDS gives vital information about a sample's chemical makeup and element distribution. It is widely used in a variety of scientific domains including materials science, geology, biology, forensics, and semiconductor analysis.

EDS operates on the principle that when a high-energy electron beam interacts with a sample, the sample emits distinctive X-rays. These X-rays are released because of electron shell changes in the sample's atoms. The elemental composition of the sample can be established by detecting and analyzing the emitted X-rays.

Following is the working mechanism of EDS.

The SEM's high-energy electron beam interacts with the sample surface. This interaction excites the atoms in the sample, and as they return to their ground state, they release X-rays with distinct intensities.

The produced X-rays are detected using an energy-dispersive detector, which is commonly a solid-state detector or a silicon drift detector (SDD). To capture X-rays efficiently, the detector is placed near the sample surface.

Using a high-resolution spectrometer, the collected X-rays are sorted based on their energy. Each X-ray's energy is measured by the spectrometer and assigned to a corresponding elemental peak.

The detected X-rays' energy information is processed and rendered as an X-ray spectrum. Peaks in the spectrum relate to the energy levels of various elements present in the sample. Each peak's intensity is related to the abundance of the relevant element.

The X-ray spectra is examined to determine which elements are present in the sample. This is accomplished by comparing measured peak energies to known characteristic X-ray energies for certain elements. The peak intensities are also used to calculate the sample's relative elemental concentrations.

EDS can be used to develop elemental maps of the sample surface in addition to point analysis. EDS is obtained by scanning an electron beam across the sample surface.

The obtained EDS data, which includes elemental composition, concentration, and distribution information, can be analyzed, and interpreted to derive inferences about the sample's properties, such as its elemental composition, phases, impurities, and elemental distribution patterns.

4.1.4 Contact Angle Test:

The contact angle test, also known as the contact angle measurement, is a technique for determining a liquid's wetting qualities on a solid surface. It sheds light on the interaction of a liquid droplet with a surface, which is important in a variety of applications such as coating, adhesion, surface treatment, and biomaterials [26].

The contact angle is the angle created when the liquid, solid, and vapor phases meet at the three-phase boundary. It is calculated by sprinkling a droplet of the liquid of interest onto a solid surface and analyzing the droplet's form.

Following is the working mechanism of contact angle test.

Cleaning the solid substrate or surface of interest removes any impurities or residues that may alter the wetting behavior. The substrate should be flat and uniform.

Using a syringe, pipette, or automated droplet dispenser, a little amount of the liquid under inquiry is distributed onto the surface. To guarantee consistency, the droplet size should be carefully managed.

A high-resolution camera or microscope is used to observe and image the droplet and the solid surface. It is critical to acquire a good, high-contrast photograph of the droplet shape.

Dedicated software or image analysis tools are used to analyze the collected image. Based on the geometry of the droplet, the software determines the droplet border and calculates the contact angle.

The contact angle is calculated by measuring the angle between the tangent line at the three-phase boundary of the droplet and the solid surface. This measurement can be done manually or automatically with the help of software.

The contact angle value acquired is interpreted to comprehend the wetting behavior of the liquid on the solid surface. A contact angle of less than 90 degrees suggests a liquid with good wetting (spreading), while an angle larger than 90 degrees indicates a liquid with poor wetting (non-spreading).

Multiple contact angle measurements are often performed on different regions of the surface or with different droplets to assure accuracy and repeatability. This accounts for surface heterogeneity and differences in droplet location.

4.1.5 Optical Profilometry:

2D optical profilometry is a surface metrology technique for measuring and analyzing a surface's two-dimensional (2D) topography. In contrast to three-dimensional (3D) optical profilometry, which reconstructs the entire 3D surface profile, two-dimensional (2D) optical profilometry offers information about surface roughness, texture, and features in a single plane.

The operating mechanism of 2D optical profilometry is that it entails projecting structured light onto the surface and collecting reflected or dispersed light. However, the analysis in 2D profilometry is limited to a single plane, and the measurement does not provide information regarding height changes along the surface normal.

Following is the working principle of optical profilometer.

To achieve precise measurements, the optical profilometer is set up, aligned, and calibrated. This includes appropriately situating the light source, optics, and camera.

Structured light is thrown onto the surface being measured, such as fringe patterns or grids. Techniques like phase shifting, moiré patterns, and grating projection can be used to create the patterns.

Moving the sample or the optical system across the surface captures several photographs of the structured light pattern from various angles or positions.

A camera or detector captures the reflected or dispersed light from the surface. The camera captures fluctuations in intensity or phase shifts in light patterns, which carry information about the surface topography in the scanned plane.

Specialized software is used to extract surface profile information from collected photos within the scanned plane. Analyzing the interference patterns, calculating phase shifts, or comparing the distorted projected patterns to the captured patterns are all part of this process.

A 2D surface profile is generated based on the gathered data and analysis, representing variations in height or surface features along the scanned plane. The profile is usually represented as a line or cross-section plot.

Using various tools and software, the rebuilt 2D surface profile can be further analyzed and visualized. Quantifying surface roughness characteristics, analyzing surface features, comparing samples, and doing statistical analysis are all examples of this. To comprehend the surface, the resulting 2D surface profile data is interpreted.

4.1.6 Tafel Plot Analysis

Tafel plot analysis is a technique used in electrochemistry to investigate the kinetics of electrochemical reactions and to discover critical parameters such as reaction rate, exchange current density, and electrochemical reaction processes. To analyze the behavior of an electrochemical system, plot the current density (logarithmic scale) versus the applied voltage.

Following is the working mechanism of the test.

A working electrode, a reference electrode, and a counter electrode are used to construct an electrochemical cell. Typically, the working electrode is the substance or surface under research.

Depending on the experiment, the cell is subjected to controlled potential or controlled current conditions. The applied potential is changed across a particular range while the resulting current density is monitored.

The recorded current density values are plotted against the corresponding applied potentials on a logarithmic scale. The Tafel plot is often displayed as a

linear relationship on the plot, which aids in the analysis of electrochemical behavior.

The Tafel plot has linear sections whose slopes match to the Tafel constants in the Tafel equation. Calculating the tangent to the linear component of the plot yields the Tafel slope, which measures the rate of the electrochemical process.

Tafel slope analysis offers information on the reaction mechanism and the rate-determining phase of the electrochemical process. The intercept of the Tafel plot with the current density axis can also be used to calculate the exchange current density.

The Tafel plot characteristics collected, such as the Tafel slope, exchange current density, and overpotential, are interpreted to understand the kinetics of the electrochemical reaction, the efficiency of the electrochemical system, and the overall performance of the electrochemical system [16].

4.1.7 Optical Microscopy:

Optical microscopy is a popular technique for studying transparency in a variety of materials. It enables the observation and investigation of light transmission through a sample, providing significant information about its optical qualities and transparency. Depending on the needs of the investigation, optical microscopy can be performed using a variety of microscopes, including brightfield, darkfield, phase contrast, and polarized light microscopy.

The optical microscopy working principle is lighting a sample with visible light and studying the interaction of light with the sample. Depending on the sample's transparency and optical qualities, light can be transmitted, absorbed, dispersed, or refracted. The lighting is optimized by microscope optics, which include the objective lens, condenser, and light source.

Following is the working mechanism of optical microscopy.

The material of interest is ready for microscope examination. Mounting the sample on a glass slide, thinning it to an acceptable thickness, or utilizing

specialized sample preparation processes based on the individual requirements may be required.

The microscope is set up and oriented for viewing transparent samples. This includes choosing the best objective lens, changing the condenser location, and optimizing the illumination intensity and angle.

A visible light source, such as a halogen bulb or an LED, is used to illuminate the sample. The light is focused onto the sample by the condenser, which ensures appropriate illumination.

The objective lens captures and magnifies the light emitted through the material. The light is caught by a camera or transmitted through the eyepiece for visualization and analysis. To achieve clear and detailed images, the observer can change the focus and magnification.

The observed images are analyzed to determine the sample's transparency qualities. This could include qualitative analysis, such as assessing overall transparency or identifying specific qualities or flaws. Quantitative analysis can also be accomplished by employing specialized software or image analysis techniques to measure factors such as light transmission, contrast, or refractive index.

Transparent samples can be compared to reference samples or other samples under different conditions. This enables the evaluation of modifications.

4.1.8   Wear Resistance Test

Testing for wear resistance is a technique used to assess a material or coating's resistance to wear, abrasion, or friction-related damage. In several fields, including manufacturing, automotive, aerospace, and materials science, it is crucial to evaluate materials and surface treatments to determine their performance and durability.

A typical technique for assessing the wear resistance and frictional qualities of materials is the pin-on-disk test. It entails carefully controlled sliding of a pin- or ball-shaped sample against a revolving disc made of a different substance. The

test yields important insights into the material's resistance to wear and frictional behavior.

The idea of sliding friction underlies the pin-on-disk test's operation. A rotating disc formed of a different substance is forced up against a pin-shaped sample, which is frequently cylindrical or spherical in shape. The pin is put under a specific load, and when the disc rotates, the pin and disc surface move relative to one another.

The desired specifications are followed in the preparation of the pin and disc samples. The pin sample is made of the material under inquiry and is often smaller in size. The counter-surface is typically the larger, more diversely constructed disc sample.

To enable controlled application of the standard load, the pin sample is mounted in a holder or fixture. The test involves precisely rotating the disc sample, which is mounted to a spinning spindle.

The pin sample is subjected to the desired load, typically using a mechanical or hydraulic system. To accurately represent the contact pressures encountered in the intended application, the load is carefully chosen.

The pin slides across the disc surface when the disc is configured to rotate at a constant speed. You can change the rotating speed to reflect operating circumstances.

Pin-on-disk tests are conducted for a predetermined length of time or number of cycles. Depending on the test's goals, the qualities of the material, and the expected wear pattern, the duration may change.

During the test, several characteristics, such as the frictional force, wear volume, wear depth, or coefficient of friction, can be observed and recorded. The wear resistance and frictional properties of the material are revealed by these measures [46].

4.1.9 Scratch test

The scratch test is a popular technique for determining a material's hardness, stickiness, and scratch resistance. It entails moving a pointed or sharp stylus

across the surface of the material being studied while imparting a controlled force or load on it. The test yields important insights on the material's overall durability and scratch resistance.

The scratch test is based on the idea of applying controlled damage to the surface of the material with a pointed or sharp indenter. To assess the material's scratch resistance, the applied force results in deformation, material removal, or surface damage that may be visually observed and quantitatively analyzed.

Following is the working mechanism of the scratch test.

Making sure the testing surface is spotless and flat prepares the sample. To accomplish this, the surface may need to be polished, grounded, or prepared in accordance with needs [47].

The scratch test apparatus is set up for the test, which commonly consists of an indenter or stylus, a loading mechanism to impart the appropriate force, and a way to regulate the stylus' movement across the test sample surface.

Using a loading mechanism, a certain force or load is applied to the stylus. Depending on the test's goals and the qualities of the material, the force might be delivered continuously or progressively.

The speed and velocity of the stylus are controlled as it travels across the sample surface. Depending on the needs of the test, the stylus may be moved in a straight line or along a predetermined path. The force and motion parameters are chosen to mimic the intended use or to test the scratch resistance of the material in various scenarios.

During the test, the material's surface response is scrutinized. As the stylus meets the surface, it is important to keep an eye out for any obvious scratches, material deformation, chipping, or cracks. To record and examine the scratch behavior, high-resolution imaging methods or real-time imaging methods may be used.

To determine the material's scratch resistance and hardness, recorded data is analyzed, such as scratch depth, width, or appearance. To evaluate the

performance of the material, the data can be compared to references or standards.

RESULTS AND DISCUSSION

5.1 Introduction

To determine the right composition and structure of our manufactured samples, many characterization procedures were applied. This chapter looks at the outcomes for all the samples that were examined, and it also includes a commentary of the outcomes.

5.1.1   Characterization of the Synthesized Powder

5.1.1.1   FTIR of MF resin:

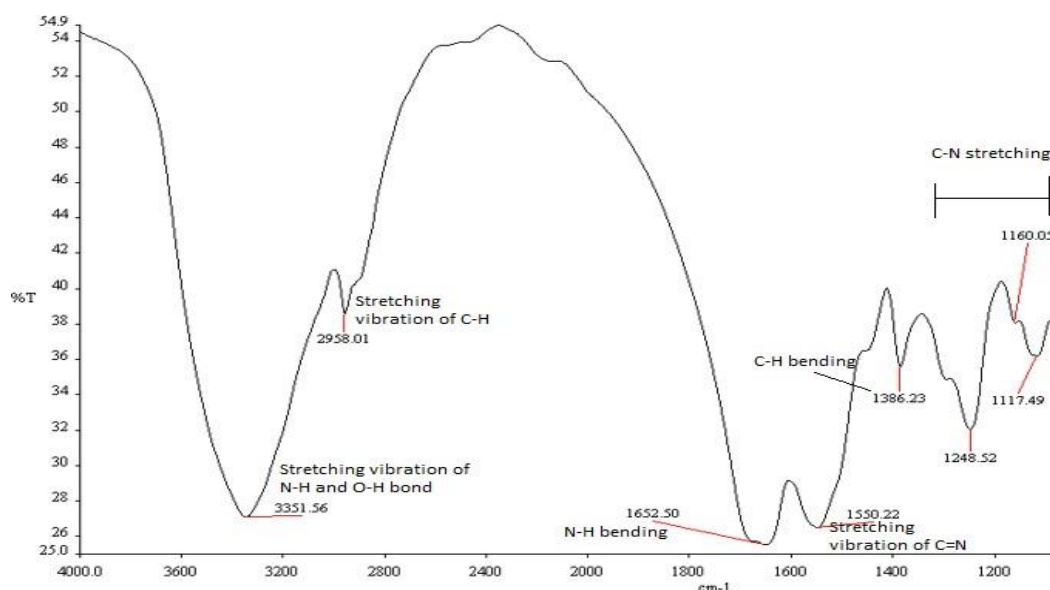Below is the FTIR result of the synthesized powder.

Figure 20, FTIR of MF powder.

Here we can see that the desired functional groups are present. At wavenumber 3351 cm^{-1}, we have stretching vibration of N-H group of amine and O-H group of the alcohol. At 2958 cm^{-1}, we have stretching vibration of C-H bond indicating the presence of alkane group. Then at 1652 cm^{-1}, we see a peak representing the N-H bending of amine. Then we have the peak of C=N confirming the presence of heterocyclic nitrogen at 1550 cm^{-1}. After that, there is a peak at 1386 cm^{-1}, indicating that there is C-H bending of the aldehyde group. Lastly, we observe

three peaks, from 1248 cm^{-1} to 1160 cm^{-1} showing the stretching vibration caused by C-N of the amine group [2].
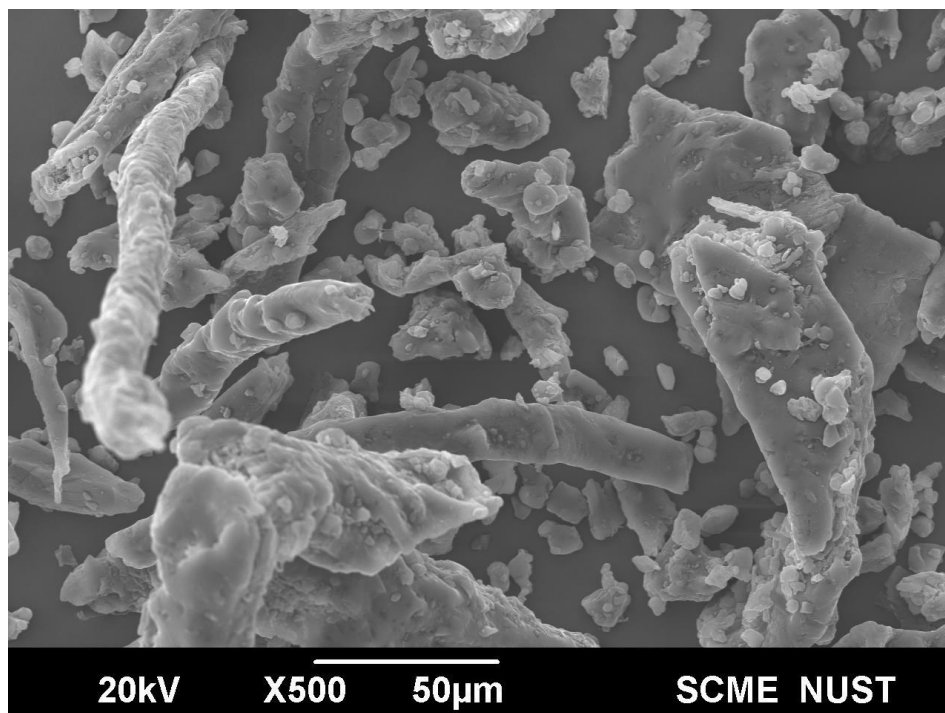
5.1.1.2 SEM of MF powder:

Figure 21, SEM of MF powder.

Here are the SEM results of the powder synthesized. As we can see, there are irregularly shaped rods, particles, and sheets present. Overall, there is seen mixed morphology of the powder. The morphology of the powder does not affect our results. It is because the powder is not being used in the direct application, rather we are going to make its solution/suspension with DMSO. So, the powder particles shape is not strictly required to be spherical. Ideally, the particles should be spherical but that requires high operating conditions along with even comminution. Such results are due to the uneven crushing of the powder leading to such uneven and irregular shaped particles.

5.1.1.3 EDS results:

The energy dispersive spectrometry was done to determine the composition of the powder. We need to find the composition for multiple reasons. One of the reasons is to know that there is no foreign particle or element which is bonded with the original chain or structure. We would not like that to happen because the functionality of the polymer decreases. Secondly, we need to the EDS results

to check if there is any contamination in the synthesized powder. The contamination could also have adverse effects on the structure and functionality. Lastly, from the reactions being conducted, we wanted to know if there are salt particles formed and attached with the main powder. We wanted to avoid that from happening since salts like NaCl provide hydrophilic effect and our coating would not be able to provide a good contact angle if the salt particles were present.

The results showed that only carbon, nitrogen, and oxygen were present. The hydrogen could not be detected because of its small sized atom. We could see that carbon is present around 33.7 wt.% with nitrogen being 34.7% and lastly oxygen at 31.6 wt. %. These amounts lie in the optimum range.

The result of the EDS tells us that the MF resin synthesized is of high purity.

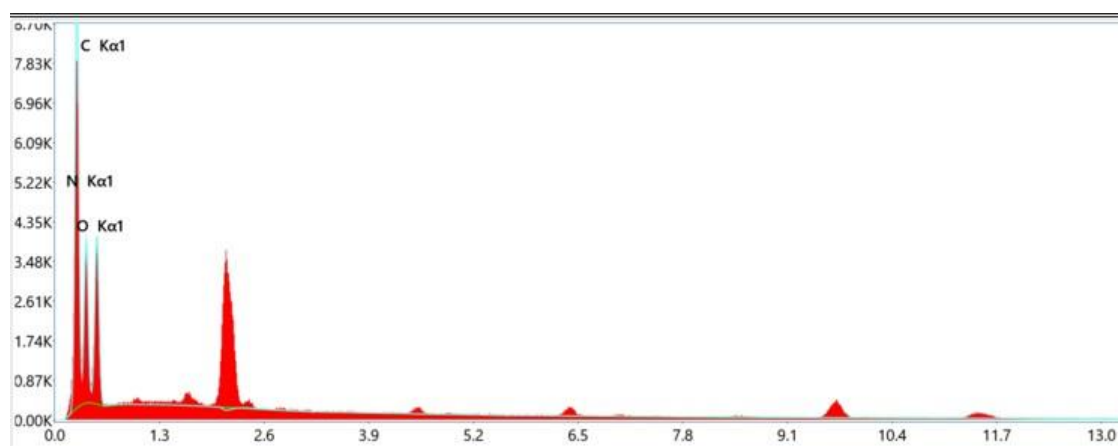*Figure 22, EDS of MF resin.*

Element	Weight %	MDL	Atomic %
C K	33.7	0.16	38.7
N K	34.7	0.54	34.1
O K	31.6	0.44	27.2

Figure 23, Elemental percentages in MF resin.

5.1.2 Characterization of the Coating

5.1.2.1 Optical Profilometry:

2D optical profilometry was done to determine the thickness of the coating we developed. We needed to achieve the minimum possible thickness from the EPD testing by the optimization of all the parameters. Initially, with parameters too low, we were getting a very thin layer but the problem with that coating was that it was neither uniform nor it had good adhesion to the surface of the substrate. We needed to develop a coating which exhibits good adhesion and other properties too. For that purpose, after the optimization of the parameters, we were able to achieve the proper coating at 60 V for 120 seconds. It provided us coating thickness of 7.63 μm. The limitations defined by the automotive industry tell us that the coating thickness developed over the body of the vehicle should be less than 50 μm. We were able to meet their requirements as well.

Second comes the surface roughness of the coating over the substrate. We need to have smooth coating over the substrate to maintain the integrity of the surface. Rough surface over the car body is not desired at all. We need to have a surface which is smooth in nature too. This issue would have caused the paint to give a texture surface on the car body which is highly undesirable. So, after the optimization of all the parameters and preheating the substrate for few minutes before the application of coating led to the provision of a smooth coating with an average roughness of 1.04 μm. The coating roughness is also defined by the automotive industry which states that the thickness should be around 1 μm. We were successful in meeting the desired roughness too.
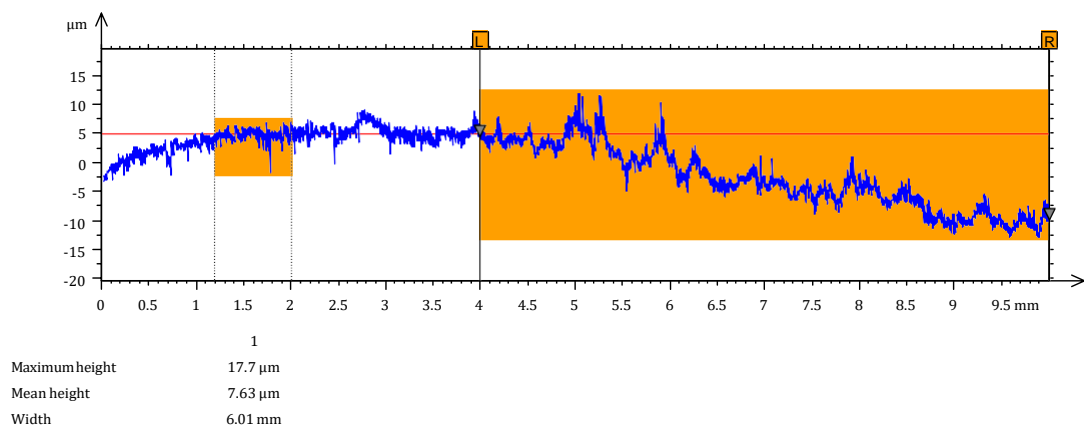

Maximum height	17.7 μm
Mean height	7.63 μm
Width	6.01 mm

Figure 24, Optical profilometry of the coating.

5.1.2.2   Wetting Characteristics:

The wettability of the coating is the most crucial and integral part of the whole project. We were required to achieve contact angle of more than 150°. There are three contact angle results shown below. The first result was achieved when the contact angle test was performed on the bare or uncoated mild steel substrate. It was done to check how much increase was required to achieve. The bare sample was just cleaned with ethanol and after drying, the test was conducted. The result was a very low angle of 39° which shows that the bare mild steel is highly hydrophilic in nature [32].
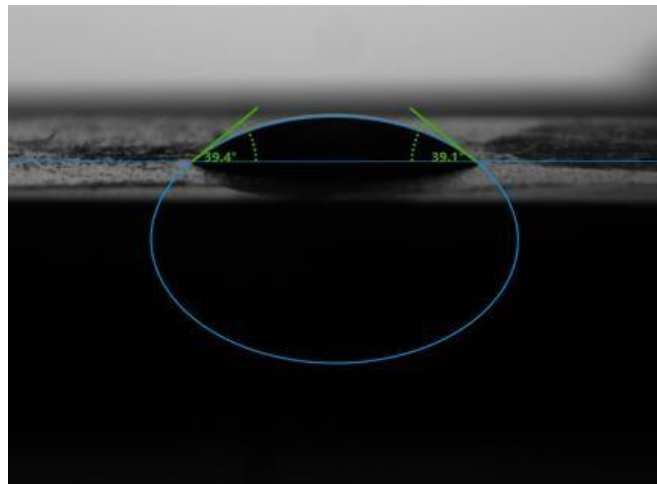

Figure 25, Contact angle on bare sample.

The second test was conducted by coating the MF resin over the substrate of mild steel. This test was done to study the wetting characteristics of the steel sample with only resin coating. We needed to know how much angle we were supposed to increase by the addition of nanoparticles to make it superhydrophobic. The second test gave us a contact angle of 116° showing that the melamine formaldehyde alone is hydrophobic in nature.

Figure 26, Contact angle of MF coated sample.

The last test was done on the final coating material, coated over the MS substrate. This coating material was the composite of melamine formaldehyde and silica nanoparticles. After the adjustment of silica nanoparticles, we ended up going for 0.6 wt.% which gave us a contact angle of 148°. By further addition of silica nanoparticles, significant increase in the contact angle was not being observed. So, we got a final coating giving us almost superhydrophobic contact angle.
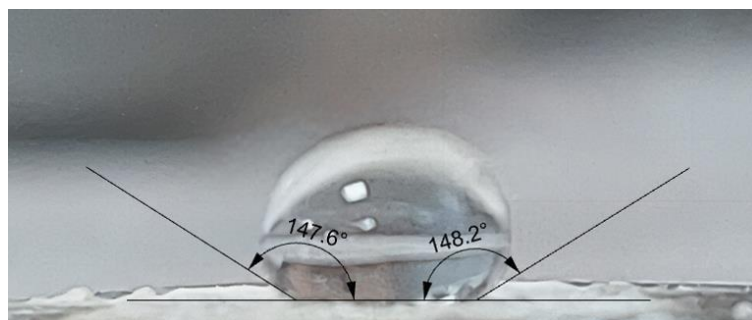

Figure 27, Contact angle of MF and silica coated sample.

5.1.2.3   Tafel Plot Analysis:

The Tafel plot analysis was done to study the corrosion behavior of the coating. We needed to make sure that the contents of the coating were not adversely affecting the steel substrate. Sometimes, the coating deposited over the substrate starts to corrode the sample after some time. We needed to make sure that the MS substrate is safe with the coating being deposited. For that purpose, we conducted the test by taking two samples, one was the bare uncoated sample while the other was deposited with the composite of the melamine formaldehyde

and silica nanoparticles. Both were tested under the same conditions, at room temperature, with 3.5% NaCl solution. The Icorr value achieved by uncoated sample was 57.90 μA while for the coated sample, we got 539.0 pA. There was a great difference in these values. Similarly, the Ecorr value for the uncoated sample was seen to be -937 mV while for the coated sample, it was -452 mV. Lastly, we have the overall corrosion rate for the uncoated sample was seen to be 35.33 mpy while for the coated sample it was 328.6×10^{-6} mpy. There is a huge difference between these two results. These tests show us that coating developed is highly corrosion resistant in nature.
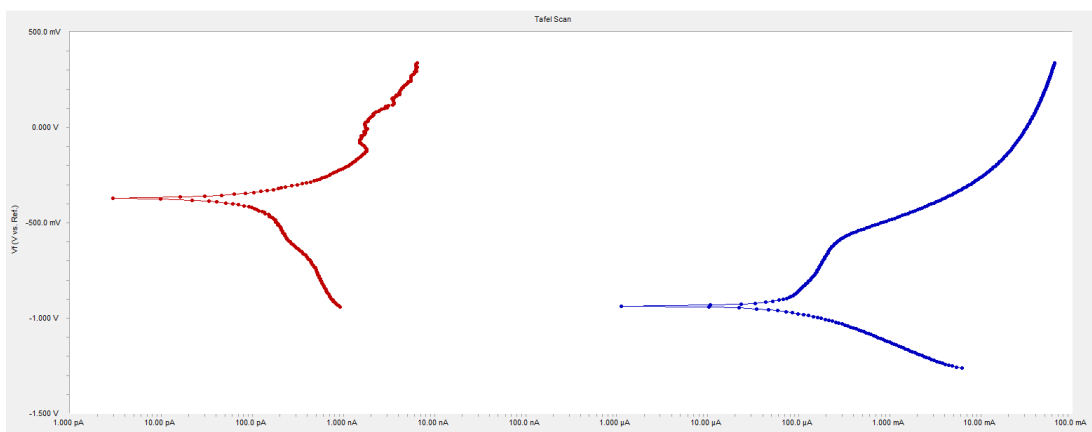
	Uncoated Mild Steel	Coated Mild Steel
Icorr	57.90 μA	539.0 pA
Ecorr	-937.0 mV	-452.0 mV
Corrosion Rate	35.33 mpy	328.6×10^{-6} mpy

Figure 28, Tafel plot of coated vs uncoated sample.

5.1.2.4 Optical Microscopy:

Optical microscopy was done to study the transparent nature of the coating. This analysis was done to confirm that the coating being developed is transparent in nature because it was one of the goals of the project to do so. To do so, again we took two samples, one was uncoated which we took as a reference and the other was the coated sample. Both samples were observed under an optical microscope at 200X. Scratches are more visible in the uncoated sample. These scratches were intentionally introduced to provide sufficient roughness to the surface of the substrate for better adhesion of the coating. On the other hand, we have coated samples, where scratches are less visible. It is because the resin has

somewhat filled scratches by entering them. Overall, if we compared the two images, we see that they both have same color which tells us that the coating deposition has not changed the color of the surface. From these results, we could say that the coating is transparent in nature.
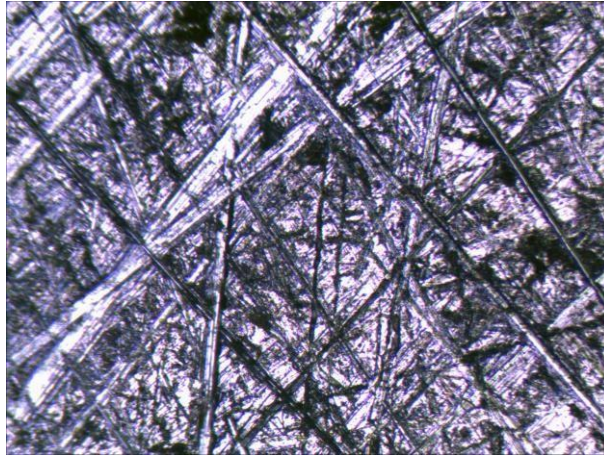

Figure 29, Microscopy of uncoated sample.
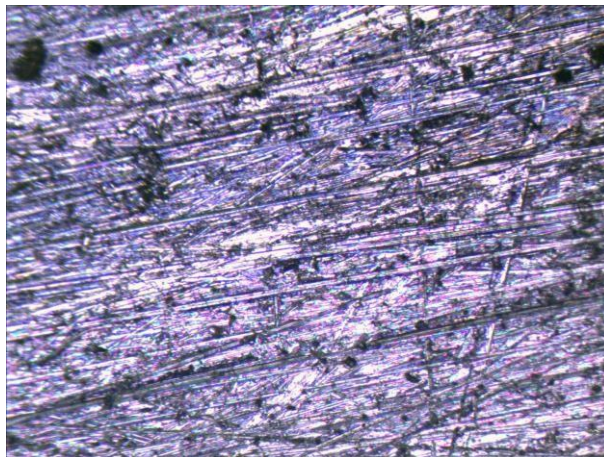
Figure 30, Microscopy of coated sample.

5.1.2.5   Wear Resistance Test:

Our objective is to develop a wear resistant coating which would not be easily deteriorated. Wear resistant coating increases the ability of the surface to become more immune to mild attacks by environmental factors. So, for that reason, we performed wear resistance test under the ASTM standard G99.

According to that, we prepared the sample by coating the sample over a circular steel substrate. Then we applied a preload of 100 N with a speed of 1 rev/min and the test lasted for 60 seconds. The temperature was not changed, and room

temperature was used. As a result, we got a friction coefficient of 0.079. The value is very small, and we know that the lower the value of friction coefficient, greater the surface is wear resistant. The value of friction coefficient, less than 0.1, is considered exceptional. Below is a graph between the frictional force and the time for building a correlation. We were successful in achieving good wear resistant coating.
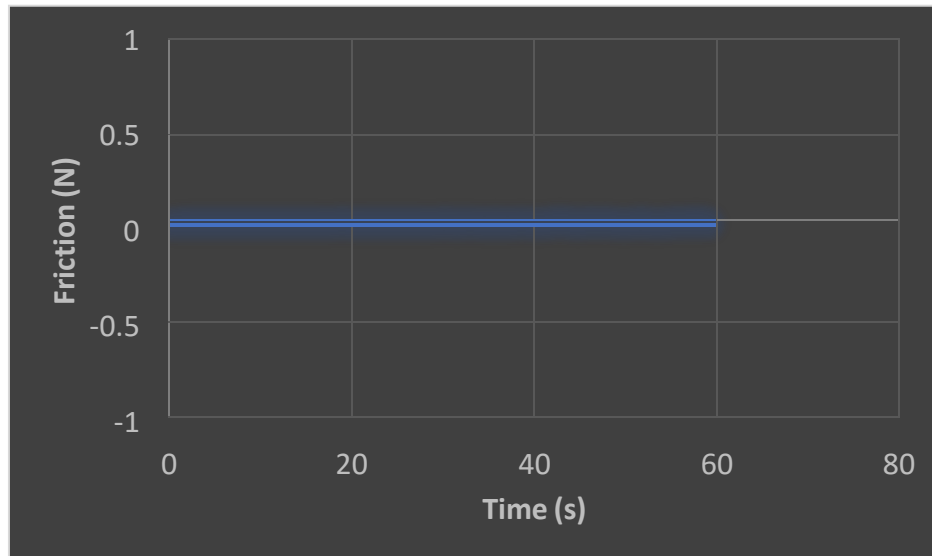

Figure 31, Friction vs time graph.

Preload(N)	100	Spindle speed (r/min)	1
Time(s)	60	Revolutions	1
Temp(°C)	26.7	Friction(N)	0.03
Friction Coefficient	0.079		

Figure 32, Set conditions for the wear test and the friction value obtained.

5.1.2.6 Scratch Test:

Scratch test was performed to check the scratch resistance of the coating deposited. Wear resistance is a measure of major forces acting on the surface, but scratch test gives us the results of small forces acting in a concentrated manner over a small area. The test was done to ensure the durability of the coating developed. For that reason, coating was deposited over the steel sample and the needle was allowed to run for the given length with load being applied over it. We used four loads. The coating showed no scratch for the load of 100 g. When the load was increased to 200 g, the needle ran over the surface with a less smooth manner as compared to the load of 100 g. At load of 400 g, we saw that

the coating was getting penetrated by the needle but could not develop a scratch. Finally, at the load of 500 g, a proper scratch was produced which was penetrated by the needle reaching the steel surface.

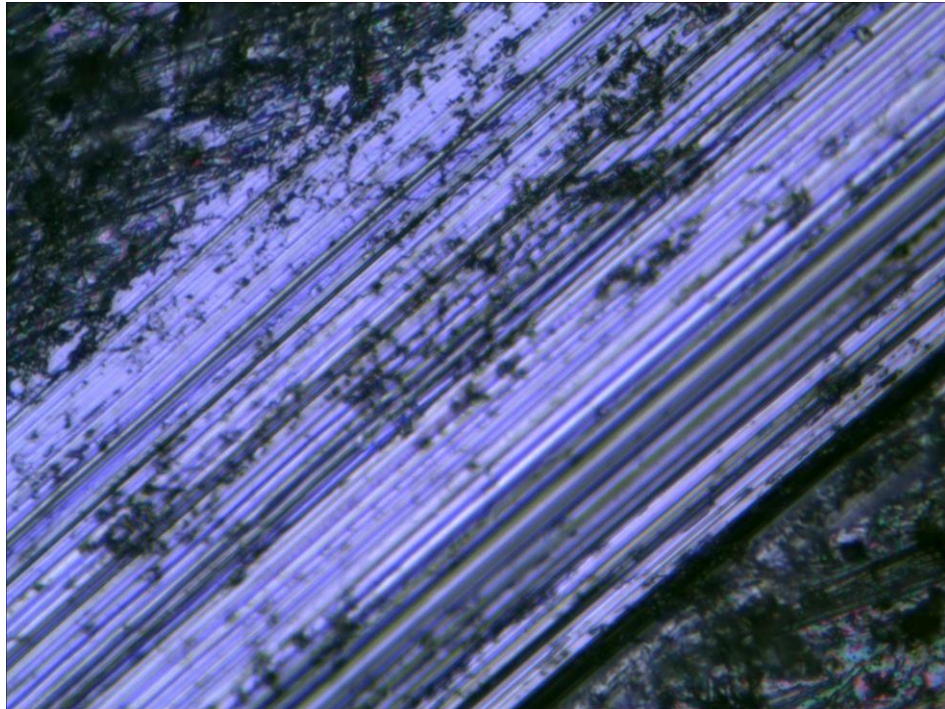Here is also an optical image of the scratch caused by the load of 500 g, at 500x.

Figure 33, Scratch on the coated sample by 500 grams of force.

CONCLUSION AND REFERENCES

Conclusion

The powder's composition as MF (the precise identity of "MF" is not mentioned) was validated by analysis utilizing FTIR (Fourier Transform Infrared Spectroscopy). This method made it possible to identify the functional groups and chemical bonds that were present in the powder, giving important details about its molecular structure.

The measurement of the coating's contact angle, which establishes the angle between a liquid droplet and a solid surface, showed a startling rise of about 300%. The coating has now reached a superhydrophobic condition, which means it repels water very well, as evidenced by the considerable rise. Numerous practical uses for this characteristic include self-cleaning surfaces and effective water resistance. The transparency of the coating was evaluated and verified using optical microscopy. This characterization method made it possible to see the microstructure of the coating and proved that it does not hinder light. In applications where maintaining optical clarity is essential, like protective coatings for windows or display screens, the coating's transparency is a key component.

A Tafel plot comparison between the coated and untreated samples was done to evaluate the coating's corrosion resistance. Tafel plots are used to examine materials' corrosion rates and other electrochemical properties. Comparing the samples showed that the coated sample had significantly better corrosion resistance than the untreated sample. This result shows that the coating effectively protects against corrosion's harmful effects, which can increase the lifespan of coated materials in corrosive settings.

The coated sample showed outstanding wear resistance in addition to corrosion resistance. The extremely low friction coefficient found proved this. The coating's capacity to resist wear and lessen friction-related damage is indicated by its low friction coefficient, which shows that it encounters little resistance

when in touch with other surfaces. In applications where longevity and durability are crucial, such as protective coatings for machinery components or high-stress surfaces, this feature is extremely desirable.

In conclusion, the Tafel plot comparison, optical microscopy, friction coefficient assessment, and FTIR analysis and characterization of the powder have all contributed to a thorough understanding of the characteristics and performance of the coating. This coating is a highly promising material with a wide range of potential applications due to its proven composition, superhydrophobic nature, transparency, great corrosion resistance, and exceptional wear resistance.

Future Prospects

Enhanced electrophoretic deposition and Application of organic solvents

The electrophoretic deposition (EPD) technique can be further investigated in the future to improve its use in the deposition of superhydrophobic transparent coatings. The research can go further into the optimization of EPD parameters including voltage, deposition time, and suspension concentration by looking into the usage of DMF (dimethylformamide) as a solvent base. Through testing, it may be possible to manage the coating's porosity, thickness, and surface shape more precisely, ultimately improving the coating process's effectiveness and performance. Research on n-Butylated Melamine Formaldehyde Resin for Automotive Applications is a promising future development [27].

The investigation of n-butylated melamine formaldehyde resin as a viable coating material for automotive applications is another direction for future study. The project can study the possible advantages of this resin in terms of improved hydrophobicity, adhesion, durability, and resistance to environmental variables by examining the synthesis, characteristics, and performance of this resin. This work can help increase the variety of coating materials that are available for automotive applications, giving researchers more possibilities for creating transparent, superhydrophobic coatings with improved performance properties [11].

Investigating nanoparticles for formaldehyde emission reduction

Future research can concentrate on investigating the integration of nanoparticles in the coating formulation to lower formaldehyde emissions considering the rising significance of environmental sustainability. The project can attempt to limit or eliminate the release of formaldehyde during the coating application and curing process by investigating the use of ecologically friendly nanoparticles, such as silica nanoparticles or other suitable substitutes. In line with the growing demand for environmentally friendly solutions in the automotive industry, this study may help produce more environmentally friendly coatings [30].

Possibility of using resin composite in spray and dip coatings

Future study can concentrate on examining the produced resin composite's appropriateness for spray and dip coatings on composite materials, broadening the application range. Considering their light weight and great strength, composite materials are being employed more and more in the production of automobiles. The study can aid in the creation of protective coatings for composite vehicle parts by investigating the compatibility and performance of the resin composite in coating composite substrates [27]. This study may provide important information about the coating's adherence, resilience, and capacity to resist corrosion on composite surfaces, creating new opportunities for its use in the automotive sector.

The research can increase knowledge and use of superhydrophobic transparent coatings for automotive applications by further investigating these potential future uses. These study fields may result in advancements in coating procedures, material choices, environmental sustainability, and compatibility with new automotive materials, which may ultimately aid in the creation of sophisticated coatings for improved automobile performance and defense.

REFERENCES

1. Dorieh, A., Farajollah Pour, M., Ghafari Movahed, S., Pizzi, A., Pouresmaeel Selakjani, P., Valizadeh Kiamahalleh, M., Hatefnia, H., Shahavi, M.H. and Aghaei, R. (2022). A review of recent progress in melamine-formaldehyde resin-based nanocomposites as coating materials. *Progress in Organic Coatings,* https://doi.org/10.1016/j.porgcoat.2022.106768.

2. Merline, D.J., Vukusic, S. and Abdala, A.A. (2012). Melamine formaldehyde: curing studies and reaction mechanism. *Polymer Journal*, 45(4), pp.413–419. https://doi.org/10.1038/pj.2012.162.

3. Cremaldi, J. and Bhushan, B. (2018). Fabrication of bioinspired, self-cleaning superliquiphilic/phobic stainless steel using different pathways. *Journal of Colloid and Interface Science*, 518, pp.284–297. https://doi.org/10.1016/j.jcis.2018.02.034.

4. BESRA, L. and LIU, M. (2007). A review on fundamentals and applications of electrophoretic deposition (EPD). *Progress in Materials Science*, 52(1), pp.1–61. https://doi.org/10.1016/j.pmatsci.2006.07.001.

5. Schaeffer, D.A., Polizos, G., Smith, D.B., Lee, D.F., Hunter, S.R. and Datskos, P.G. (2015). Optically transparent and environmentally durable superhydrophobic coating based on functionalized SiO2 nanoparticles. *Nanotechnology*, [online] 26(5). https://doi.org/10.1088/0957-4484/26/5/055602.

6. Meena, M., Balraj Krishnan Tudu, Kumar, A. and Bhushan, B. (2020). Development of polyurethane-based superhydrophobic coatings on steel surfaces. 378(2167),pp.20190446–20190446. https://doi.org/10.1098/rsta.2019.0446.

7. Sas I, Gorga R E, Joines J A and Thoney K A 2012 Literature review on superhydrophobic self-cleaning surfaces produced by electrospinning *J. Polym. Sci. B* **50** 824–45

8. Polizos G, Tuncer E, Qiu X F, Aytug T, Kidder M K, Messman J M and Sauers I 2011 Nonfunctionalized polydimethyl siloxane superhydrophobic surfaces based on hydrophobic–hydrophilic interactions *Langmuir* **27** 2953–7

9. Weng C J, Peng C W, Chang C H, Chang Y H and Yeh J M 2012 Corrosion resistance conferred by superhydrophobic fluorinated polyacrylate-silica composite coatings on cold-rolled steel *J. Appl. Polym. Sci.* **126** E48–55

10. Hamaker HC. Formation of deposition by electrophoresis. Trans Farad Soc 1940;36:279–83.

11. Troelstra SA. Applying coatings by electrophoresis. Philips Tech Rev 1951;12:293–303.

12. Anil, K. & Vimal, K. Modelling and experimental investigation of melamine formaldehyde polymerization. Macromolecules 23, 3729–3736 (1990).

13. Mijatowic, J., Binder, W. H., Kubel, F. & Kantner, W. Studies on the stability of MF resin solutions: investigations on network formation. Macromol. Symp. 181, 373–382 (2002).

14. Wilson, R. C. & Pfohl, W. F. Study of cross-linking reactions of melamine/formaldehyde resin with hydroxyl functional polyester by generalized 2-D infrared spectroscopy. Vibrat. Spect. 23, 13–22 (2000).

15. Manfred, R., Hartmut, B., Sergey, I., Valery, P., Paul, L. & Primachenko, O. N. The reaction mechanism of the transetherification and crosslinking of melamine resins. Macromol. Symp. 217, 431–443 (2004).

16. Anonymous. 2005 In Corrosion of metals and alloys-electrochemical test methods-guidelines for conducting potentiostatic and potentiodynamic polarization measurements, ISO 17475:2005. Washington, DC: American National Standards Institute.

17. Nanda D, Varshney P, Satapathy M, Mohapatra SS, Bhushan B, Kumar A. 2017 Single-step method to fabricate durable superliquiphobic coating on aluminum surface with self-cleaning and anti-fogging properties. J. Colloid Interface Sci. 507, 397–409.

18. Ahmad, S., Ashraf, S.M., Kumar, G.S., Hasnat, A. and Sharmin, E. (2006). Studies on epoxy-butylated melamine formaldehyde-based anticorrosive coatings from a sustainable resource. *Progress in Organic Coatings*, [online] 56(2), pp.207–213. https://doi.org/10.1016/j.porgcoat.2006.05.002.

19. Ahmadi, Z. (2019). Epoxy in nanotechnology: A short review. *Progress in Organic Coatings*, 132, pp.445–448. https://doi.org/10.1016/j.porgcoat.2019.04.003.

20. Bauer, D.R. (1986). Melamine/formaldehyde crosslinkers: characterization, network formation and crosslink degradation. *Progress in Organic Coatings*, 14(3), pp.193–218. https://doi.org/10.1016/0033-0655(86)80001-2.

21. Pissis, P. (2007). *Thermoset Nanocomposites for Engineering Applications*. [online] *Google Books*. iSmithers Rapra Publishing. Available at: https://books.google.com.pk/books?hl=en&lr=&id=uGyekcHA5AMC&oi=fnd&pg=PR9&ots=eklLUZDT89&sig=nSkUELvbUqtSdOX903X1etteYE4&redir_esc=y#v=onepage&q&f=false [Accessed 7 Jun. 2023].

22. Vo, T.D.T., Himmelsbach, M., Haunschmidt, M., Buchberger, W., Schwarzinger, C. and Klampfl, C.W. (2008). Improved analysis of melamine–formaldehyde resins by capillary zone electrophoresis–mass spectrometry using ion-trap and quadrupole-time-of-flight mass spectrometers. *Journal of Chromatography A*, [online] 1213(1), pp.83–87. https://doi.org/10.1016/j.chroma.2008.07.002.

23. Li, T., Cao, M., Zhang, B., Yang, L. and Du, G. (2018). Effects of Molar Ratio and pH on the Condensed Structures of Melamine-Formaldehyde Polymers. *Materials*, 11(12), p.2571. https://doi.org/10.3390/ma11122571.

24. R. Nastke, Dietrich, K., Reinisch, G., Rafler, G. and Gajewski, H. (1986). The Initial Stage of the Reaction of Melamine with Formaldehyde. 23(5), pp.579–596. https://doi.org/10.1080/00222338608058497.

25. Okano, M. and Ogata, Y. (1952). Kinetics of the Condensation of Melamine with Formaldehyde. 74(22), pp.5728–5731. https://doi.org/10.1021/ja01142a047.

26. Khajouei, M., Peyman Pouresmaeel-Selakjani and Latifi, M. (2021). Spectroscopy and Other Miscellaneous Techniques for the Characterization of Bio- epoxy Polymers, Their Blends, and Composites. https://doi.org/10.1002/9783527823604.ch9.

27. Ahmad, S., Ashraf, S.M., Kumar, G.S., Hasnat, A. and Sharmin, E. (2006). Studies on epoxy-butylated melamine formaldehyde-based anticorrosive coatings from a sustainable resource. *Progress in Organic Coatings*, [online] 56(2), pp.207–213. https://doi.org/10.1016/j.porgcoat.2006.05.002.

28. Wang G Y, Wang H R and Guo Z G 2013 A robust transparent and anti-fingerprint superhydrophobic film *Chem. Commun.* **49** 7310–2

29. Lin J B, Chen H L, Fei T and Zhang J L 2013 Highly transparent superhydrophobic organic-inorganic nanocoating from the aggregation of silica nanoparticles *Colloids Surf. A* **421** 51–62

30. Salthammer, T., Mentese, S. and Marutzky, R. (2010). Formaldehyde in the Indoor Environment. *Chemical Reviews*, 110(4), pp.2536–2572. https://doi.org/10.1021/cr800399g

31. A. Hooda, M.S. Goyat, J. K. Pandey, A. Kumar, R. Gupta, A review on fundamentals, constraints, and fabrication techniques of superhydrophobic coatings, Progress in Organic Coatings, Volume 142, 2020, 105557, ISSN 0300-9440, https://doi.org/10.1016/j.porgcoat.2020.105557

32. K. Sharma, A. Hooda, M.S. Goyat, R. Rai, A. Mittal, A review on challenges, recent progress and applications of silica nanoparticles based superhydrophobic coatings, Ceramics International, Volume 48, Issue 5, 2022, Pages 5922-5938, ISSN 0272-8842, https://doi.org/10.1016/j.ceramint.2021.11.239

33. Avgustinik AI, Vigdergauz VS, Zharavlev GI. Electrophoretic deposition of ceramic masses from suspension and calculation of deposit yields. J Appl Chem USSR (English Translation) 1962;35(10):2175–80.

34. Basu RN, Randall CA, Mayo MJ. Fabrication of dense zirconia electrolyte films for tubular solid oxide fuel cells by electrophoretic deposition. J Am Ceram Soc 2001;84(1):33–40.

35. Chen F, Liu M. Preparation of yttria-stabilised zirconia (YSZ) films on La0.85Sr0.15MnO3 (LSM) and LSM–YSZ substrate using an electrophoretic deposition (EPD) process. J Eur Ceram Soc 2001;21:127–34.

36. Negishi H, Yanagishita H, Yokokawa H. Electrophoretic deposition of solid oxide fuel cell material powders. In: Proceedings of the electrochemical society on electrophoretic deposition: fundamentals and applications, vol. 2002-21, Pennington, USA, 2002. p. 214–21.

37. Biesheuvel PM, Verweij H. Theory of cast formation in electrophoretic deposition. J Am Ceram Soc 1999; 82(6):1451–5.

38. West JOF, Critchlow GW, Lake DR, Banks R. 2016 Development of a superhydrophobic polyurethane-based coating from a two-step plasma-fluoroalkyl silane treatment. Int. J. Adhes.Adhes. 68, 195–204. (doi:10.1016/j.ijadhadh.2016.03.007)

39. Chen X, Yuan J, Huang J, Ren K, Liu Y, Lu S, Li H. 2014 Large-scale fabrication of superhydrophobic polyurethane/nano-Al2O3 coatings by suspension flame spraying for anti-corrosion applications. Appl. Surf. Sci. 311, 864–869. (doi:10.1016/j.apsusc.2014.05.186)

40. Yousefi E, Ghadimi MR, Amirpoor S, Dolati A. 2018 Preparation of new superhydrophobic and highly oleophobic polyurethane coating with enhanced mechanical durability. Appl. Surf. Sci. 454, 201–209. (doi:10.1016/j.apsusc.2018.05.125)

41. Vandeperre L, Van Der Biest O, Clegg WJ. Silicon carbide laminates with carbon interlayers by electrophoretic deposition. Key Eng Mater (Pt. 1, Ceramic and Metal Matrix Composites) 1997;127–131:567–73. Ma J, Chen W. Deposition and packing study of sub-micron PZT ceramics using electrophoretic deposition. Mater Lett 2002;56:721–7.

42. A.D. Çavdar, H. Yel, H. Kalaycıoˇglu, S. Hiziroglu, Effect of waste melamine impregnated paper on properties of oriented strand board, Mater. Des. 51 (2013) 751–755.

43. David, B. R. Melamine/formaldehyde crosslinkers: characterization, network formation and crosslink degradation. Prog. Org. Coat. 14, 193–218 (1986). Polym. Sci. 130 (2013) 2688–2697.

44. S. Kim, H.-J. Kim, Effect of addition of polyvinyl acetate to melamine formaldehyde resin on the adhesion and formaldehyde emission in engineered flooring, Int. J. Adhes. Adhes. 25 (2005) 456–461.

45. P. Lan, R. Yang, H. Mao, J. Cui, N. Brosse, Production of melamine formaldehyde resins used in impregnation by incorporation of ethylene glycol and caprolactam with high flexibility, storage stability, and low formaldehyde content, Bioresource 14 (2019 9916–9927).

46. Rutherford, K.L., Trezona, R.I., Ramamurthy, A.C. and Hutchings, I.M. (1997). The abrasive and erosive wear of polymeric paint films. *Wear*, 203-204, pp.325–334. doi:https://doi.org/10.1016/s0043-1648(96)07369-3.

47. AZoM.com. (2020). *Applications of Scratch Testing on Polymers*. [online] Available at: https://www.azom.com/article.aspx?ArticleID=18959#:~:text=Scratch%20testing%20is%20one%20of [Accessed 8 Jun. 2023].